École d'ingénieurs
Télécom Physique
Université de Strasbourg

Hochschule Karlsruhe
University of
Applied Sciences

Fakultät für
Informatik und
Wirtschaftsinformatik

NKIMO LENOU Randolf
Academic year 2024-2025

Double master's degree in Robotics and automation - Data Science and Artificial Intelligence

Master Thesis Report

Control of Pneumatic Turbine

19 February 2025

Company Tutor : Taraq BECHIKHI
taraq.bechikhi@airliquide.com

Academic Tutor : Franz QUINT
franz.quint@h-ka.de

Academic Tutor : Jacques GANGLOFF
jacques.gangloff@unistra.fr

Air Liquide
HEALTHCARE

Abstract

This internship is part of the feasibility studies for the INU project, aiming at designing a new emergency turbine ventilator to succeed the Monnal T60. The main actuator of this ventilator is a turbine whose speed is regulated to control the volume of air delivered or the pressure applied to the patient's lungs.

As part of my master's thesis, I worked on the development of new turbine regulation algorithms in speed, pressure, and flow. Three control strategies were explored for the inspiratory phase:

- Low-level regulation: This approach splits the control into two levels: pressure/flow and speed. I was responsible for speed regulation across various patient profiles. However, this dual regulation led to significant delays, making the strategy less effective.
- High-level regulation with adaptive PI control: This strategy relies on a PI controller with cycle-by-cycle adaptation to regulate pressure/flow. It met all the specifications.
- High-level regulation with Internal Model Control (IMC): This approach is based on an accurate process model. It is still in the testing phase, and we focused on the feasibility of this strategy for pressure/flow regulation..

In parallel, a feasibility study was conducted on an actuator for the expiratory phase, specifically a proportional valve for controlling PEEP and flow-by.

Before implementing these regulations, a signal processing phase was carried out to explore alternatives to the current moving average filter over 10 samples. Two alternatives were studied:

- A decimation filter with a reduction factor of 10.
- A combination of a Butterworth low-pass filter and a moving average.

While the latter approach provided a better-filtered signal, a 50 ms delay was observed, which could be critical for trigger detection.

This work has helped in better understanding the constraints associated with turbine regulation and in identifying the most promising strategies to ensure optimal ventilator performance.
Keywords: Turbine · Pressure · Flow · PI · IMC

Acknowledgments

As an introduction to this report, I would like to express my sincere gratitude to the entire teaching staff of the Master IRIV program and the Wirtschaftsinformatik department of HKA for their dedicated efforts and valuable support.

I would like to extend my special thanks to my internship supervisors, Mr. Taraq BECHIKHI and Mr. Mathieu ROUSSILLOT, who honored me by agreeing to guide me throughout this experience. I am deeply grateful for their cooperation, encouragement, and patience during the course of my internship. I would also like to acknowledge my academic supervisors, Mr. Franz QUINT and Mr. Jacques GANGLOFF, for their guidance and invaluable advice throughout this journey.

My gratitude also goes to the entire R&D team led by Mr. Bruno GALLONI and the Excellence in Product team led by Mr. Gilles ROBIN.

Finally, although I cannot name everyone individually, I would like to extend my warmest thanks to all the employees of Air Liquide Medical Systems, whose support and assistance enabled me to successfully complete my internship.

Contents

1 Introduction **1**
1.1 Context . . . 1
1.2 Problem Statement . . . 2
1.3 Objective of the master thesis . . . 3

2 State of the art **5**
2.1 Ventilation in the Monnal T60 . . . 5
2.1.1 Presentation and technical specifications . . . 5
2.1.2 Ventilation Operation . . . 7
2.1.3 Control Strategies Based on Ventilation Mode . . . 8
2.2 Pressure and flow regulation strategy in pulmonary ventilators . . . 10

3 Technical choices and Description of achievements **12**
3.1 Expiratory Phase Regulation . . . 12
3.1.1 Description of the Solenoid Valve . . . 13
3.1.2 Characterization of the Solenoid Valve . . . 14
3.1.3 Implemented Regulation Strategy . . . 17
3.2 Inspiratory Phase Regulation . . . 19
3.2.1 Signal Processing: Signal Filtering . . . 21
3.2.2 Strategy 1: Decoupling of Pressure/Flow Control from Turbine Speed Control . . . 27
3.2.3 Strategy 2: PI controller with cycle-by-cycle adaptation for pressure/flow rate . . . 31
3.2.4 Strategy 3: Internal Model Controller . . . 32

4 Results and Discussion **37**
4.1 Signal Processing . . . 37
4.1.1 Decimation Filter . . . 37
4.1.2 Second-Order Butterworth Filter + 10-Point Moving Average . 38
4.2 Expiratory Phase . . . 42
4.2.1 Static Analysis . . . 42
4.2.2 Dynamic Analysis . . . 42
4.2.3 PEEP Regulation . . . 43
4.3 Inspiratory Phase . . . 44
4.3.1 Decoupling Between Speed and Pressure/Flow Regulation . . 44
4.3.2 PI Controller with Cycle-by-Cycle Adaptation for Pressure/Flow Rate . . . 46
4.3.3 Internal Model Control (IMC) . . . 46

5 Conclusion and outlook **50**
5.1 Summary . . . 50
5.2 Educational Value . . . 50
5.3 Outlook . . . 50

Bibliography **51**

A Model Predictive Control for Tracking **1**

B MICADO Datasheet **4**

List of Tables

3.1 Tabulation of pressure at zero flow as a function of turbine speed . . 15
3.2 Time characteristics of the open-loop speed response 20
3.3 Time characteristics of the open-loop speed response 30

4.1 Temporal characteristics as a function of pressure 43
4.2 Slope Expiration for different PEEP levels 44
4.3 Comparison of Delay and Rise Time for Different Profiles 44
4.4 Performance Evaluation of Cycle-by-Cycle PI Regulation 46
4.5 Performance Evaluation IMC Regulation 49

List of Figures

1.1 Volume Control 2
1.2 Pressure Control 3

2.1 Monnal T60 5
2.2 Pneumatic Diagram of Monnal T60 [2] 6
2.3 Pneumatic diagram during the inspiratory phase 7
2.4 Pneumatic diagram during the expiratory phase 8
2.5 Two Stage PI Controller 9
2.6 Schematic of the proposed closed-loop system with an RLS estimator for the hose resistance estimation [6]. 10
2.7 Block Diagram of controllers [4]. 11

3.1 Current diagram of the pressure-controlled valve during a respiratory cycle 13
3.2 (3/2) Proportional solenoid valve 14
3.3 Test bench for static and dynamic characterization 15
3.4 Test bench block diagram 16
3.5 Test bench for PEEP regulation 17
3.6 Test bench block diagram for PEEP regulation 18
3.7 Flux diagram of expiratory phase strategy 19
3.8 Open-loop response of Speed to a PWM command of 4050 20
3.9 Bode diagram of the N=10 window moving average filter, Fs = 1Khz 21

3.10 Pressure and flow data over two ventilation cycles at 1 kHz. Blue: Pressure ; Red: Flow. 22
3.11 Decimation Filter 23
3.12 Frequency spectrum 25
3.13 Energy distribution by Harmonic 26
3.14 Bode diagram of Butterwoth filter 26
3.15 Decoupling of Pressure/Flow Control from Turbine Speed Control . . 27
3.16 Characteristics: Interpolated Speed, Pressure, and Flow for all speeds 28
3.17 Simulink model of the turbine's electrical section 28
3.18 Speed profile for a lung with compliance $C = 20\ L/cmH_2O$ and resistance $R = 20\ cmH_2O.s/L$ (R20C20), along with pressure and flow data. 29
3.19 Train data for turbine identification 30
3.20 Characteristics time for system identification 30
3.21 Schematic of the PI Control Scheme 31
3.22 Open-loop response of pressure to a PWM command. 33
3.23 Schematic of the IMC Scheme, inspired by [7] 33
3.24 Schematic of the IMC Implementation 36

4.1 Power spectral density of flow: Moving average filter vs. Decimation filter 37
4.2 Filtered flow sampled at 100 Hz and original flow at 1 kHz (Top: Blue - Moving average filter; Orange - Decimation filter) 38
4.3 Top: Blue - Unfiltered flow at 1 kHz; Orange - Butterworth-filtered flow at 1 kHz. Bottom: Blue - Butterworth-filtered flow at 1 kHz + 10-point moving average; Orange - 10-point moving average filtered flow. 39
4.4 Flow spectral density: Moving average filter, Decimation filter, and Butterworth filter + Moving average filter. 39
4.5 Evaluation of inspired air volume on filtered and unfiltered flow: Blue 0.388610 L (filtered flow), Red 0.388604 L (unfiltered flow), Fr = 20 bpm. 40
4.6 Comparison of inspired volume and phase shift between filtered and original flow, Fr = 60 bpm: Blue 0.70862 L (filtered flow), Red 0.70761 L (unfiltered flow). 41
4.7 Comparison of inspired volume and phase shift between filtered and original flow, Fr = 100 bpm | $f_c = 3Hz$: Blue 0.28882 L (filtered flow), Red 0.28927 L (unfiltered flow). 41
4.8 Comparison of inspired volume and phase shift between filtered and original flow, Fr = 100 bpm | $f_c = 10Hz$: Blue 0.28882 L (filtered flow), Red 0.28923 L (unfiltered flow). 41
4.9 Proximal pressure as a function of current 42
4.10 Slope of expiration 43
4.11 Comparison of expiration slopes for PEEP = 5 mbar and PEEP = 8 mbar. 43

4.12 Comparison of expiration slopes for PEEP = 12 mbar and PEEP = 15 mbar. 44
4.13 Comparison of speed and pressure profiles 45
4.14 Cycle-by-cycle PI control results 47
4.15 IMC Control Results 48

B.1 Datasheet of MICADO 4

List of abbreviations and acronyms

bpm	breaths per minute
FR	Respiratory Frequency
I/E	Inspiration/Expiration
IMC	Internal Model Control
MPC	Model Predictive Control
PCV	Pressure Control Ventilation
PEEP	Positive End Expiratory Pressure
Pi	Peak Inspiratory Pressure
PI	Proportional Integral
PSV	Proportional Solenoid Valve
PWM	Pulse Width Modulation
VCV	Volume Control Ventilation

Chapter 1

Introduction

1.1 Context

As part of the R&D department and the Hardware team, this master thesis is conducted within the framework of the INU project, which aims to design and develop a new generation of emergency pulmonary ventilators to succeed the Monnal T60. This work builds upon the final-year internships of Mohamed Ousmall and Lucas Defer. Mohamed developed a control board for a brushless motor, enabling speed control through synchronous rectification of the ventilator's turbine a design that was later refined internally. Meanwhile, Lucas focused on characterizing an electromechanical actuator for controlling the expiratory valve.

Emergency pulmonary ventilators assist or replace respiratory function in patients suffering from respiratory failure. They can operate using negative pressure applied externally to the thorax (e.g., the iron lung [1]) or, more commonly, through positive pressure applied to the airways (pneumatic or turbine ventilators). The goal of positive pressure ventilation is to maintain adequate levels of PaO2[1] and PaCO2[2] while reducing the workload on the respiratory muscles [3].

The application of positive pressure to the airways interacts with the compliance[3] of the respiratory system (lungs and chest wall), airway resistance, and respiratory system inertance, which results in gas flow to the lungs. These interactions can be expressed through the following equation of motion:

$$P_{aw} + P_{mus} = (\text{flow} \times \text{resistance}) + \left(\frac{\text{volume}}{\text{compliance}}\right) + \text{applied PEEP} + \text{auto-PEEP}$$

Where:

- P_{aw} is the airway pressure,
- P_{mus} is the pressure generated by the respiratory muscles,
- PEEP[4] is Positive End-Expiratory Pressure, whether automatic or applied.

[1] Partial pressure of O2 in arterial blood
[2] Partial pressure of CO2 in arterial blood
[3] Ability to deform = $\frac{\Delta Volume}{\Delta Pressure}$
[4] During the expiratory phase, PEEP helps expand the alveolar territory to recruit more lung areas, contributing to more efficient oxygenation

In spontaneous breathing, $P_{aw} = 0$, and the respiratory muscles provide all the pressure required for ventilation. In full ventilatory assistance, $P_{mus} = 0$, and the ventilator supplies all the pressure. In this equation of motion, the term $flow/resistance$ is expressed in units of pressure and corresponds to the resistive load. Similarly, the term $volume/compliance$, also in units of pressure, is called the elastic load. In partial assistance, both the ventilator and the respiratory muscles work together. In full assistance, the ventilator controls either the pressure or the flow (volume), introducing the two main ventilation modes: *pressure-controlled (PC)* and *volume-controlled (VC)*.

- *Volume Control (VC):* In this mode, the ventilator controls the delivered volume and imposes a respiratory rate on the patient. When a specific volume is guaranteed, the resulting pressure depends on the lung's compliance.

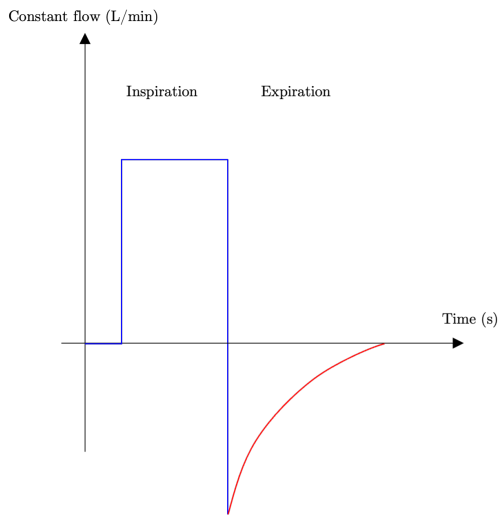

Fig. 1.1: Volume Control

- *Pressure Control (PC):* In this case, the ventilator ensures constant pressure throughout the patient's inspiratory cycle. When the pressure level is guaranteed, the delivered volume is not controlled and becomes a result, depending on the patient's compliance. Since pressure is regulated to remain constant, the flow decreases to maintain the pressure plateau (Figure 1.2).

1.2 Problem Statement

In the Monnal T60 ventilator, the primary actuator responsible for regulating airflow and pressure to the patient is a brushless motor driven turbine. This device, essential for mechanical ventilation, must be capable of adapting its regulation to suit different patient profiles, including premature infants (neonates), who require highly

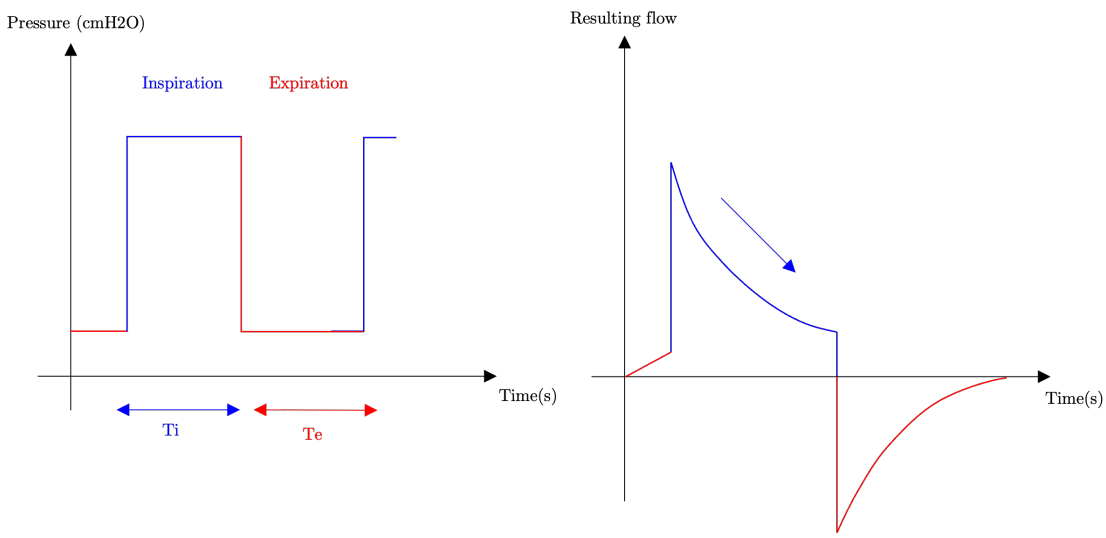

Fig. 1.2: Pressure Control

precise adjustments at high frequencies with rapid response times and no overshoot. Ensuring reliable and robust ventilation is crucial, particularly in compensating for disturbances caused by factors such as circuit compliance and resistance.

Turbine control is primarily critical during the inspiratory phase, where it must deliver precise airflow or pressure. During the expiratory phase, the turbine generates a rising flow, the performance of which is influenced by the characteristics of the patient's circuit, particularly compliance and resistance. These two parameters play a key role in the effectiveness of ventilation, making regulation highly complex due to the variability of patient profiles, unless the control algorithm is specifically adapted.

1.3 Objective of the master thesis

My master thesis focuses on developing and implementing new speed regulation algorithms for the brushless turbine to ensure airflow or pressure control for different patient groups (based on age, compliance, and resistance). The goal is to provide ventilation that meets the standards of "good ventilation" while accounting for individual patient variability.

The regulation system must meet the following requirements for each ventilation mode, in accordance with *ISO 80601-2-12* standards:

- *Pressure Control Ventilation (PCV):*
  - *Response Time:* The target pressure must be reached with a pressure slope of *120* cmH_2O/s.

  - *Stability:* Significant oscillations must be avoided.
  - *Accuracy:* The achieved pressure must remain within $\pm$*(2 cmH_2O + 4%)* of the target value.
  - *Overshoot:* Pressure overshoot must be limited to $<$ *2 cmH_2O + 4%* of the target value.

- *Volume Control Ventilation (VCV):*
  - *Response Time:* The target flow must be reached in *less than 10 ms* (from 10% to 90% of the target value).
  - *Stability:* Significant oscillations must be avoided.
  - *Accuracy:* The achieved tidal volume must remain within $\pm$*(4.0 mL + 15%)* of the target value.

Prior internal work has already led to the modeling of the ventilator (turbine), the patient circuit, and the simulation of a respiratory cycle across different patient categories (age, compliance, and resistance). My role will be to design a turbine control system capable of dynamically adjusting the turbine speed in real-time to meet these constraints and fulfill the system requirements.

Another part of my work will focus on controlling the solenoid valve responsible for regulating PEEP. The objective is to achieve complete respiratory cycle regulation while considering that the solenoid valve's control power is supplied by the turbine during its deceleration phase, corresponding to the expiratory phase.

Chapter 2

State of the art

2.1 Ventilation in the Monnal T60

2.1.1 Presentation and technical specifications

Presentation

The Monnal T60 is a turbine-based, portable ventilator designed to provide life support to infant (from 3 kg), children, and adults. It is not intended for neonatal ventilation and was developed by Air Liquide Healthcare. This ventilator helps to ventilate the patient to compensate or alleviate respiratory insufficiency. The patient contact is ensured through an appropriate interface (e.g. mask or intubation tube) that directs air from the ventilator to the lungs.

Fig. 2.1: Monnal T60

Technical Specifications

- *Tidal Volume (VT)*: 20 to 2000 mL
- *Respiratory Rate*: 1 to 80 cycles per minute
- *Inspiratory Pressure*: 5 to 60 cmH_2O

The pneumatic diagram of the T60 ventilator, illustrating the various actuators and sensors involved during the ventilation process, is shown below:

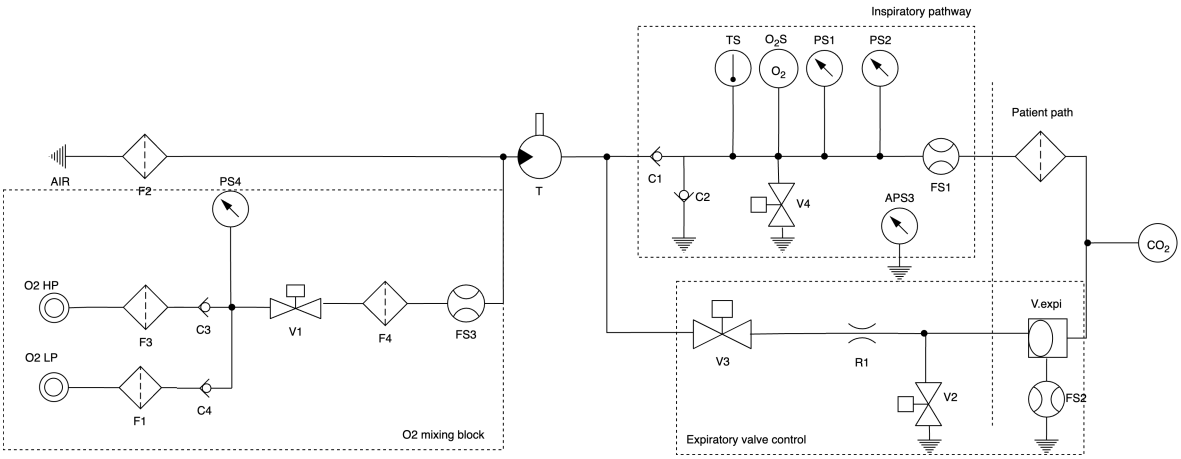

Fig. 2.2: Pneumatic Diagram of Monnal T60 [2]

Legend

AIR	Ambient air inlet
O_2 LP	Low-pressure O_2 inlet (concentrator)
O_2 HP	High-pressure O_2 inlet (network, cylinder)
V.expi	Expiratory valve equipped with a membrane
C1	Check valve
C2	Check valve
C3	Check valve
C4	Check valve
F1	O_2 inlet filter (O_2 concentrator)
F2	Air inlet filter (HEPA filter)
F3	O_2 inlet filter (compressed gas)
F4	Bronze filter (flow lamination)
FS1	Patient flow sensor
FS2	Hot-wire expiratory flow sensor
FS3	O_2 flow sensor
CO_2S	Carbon dioxide sensor (optional)
PS1	Inspiratory pressure sensor of airways
PS2	Inspiratory pressure sensor of airways (redundancy)
APS3	Atmospheric pressure sensor
PS4	O_2 pressure sensor
T	Turbine
TS	Patient gas temperature sensor
V1	Proportional valve for oxygen regulation
V2	Proportional valve for PEEP regulation
V3	All-or-nothing valve for pause execution
V4(*)	All-or-nothing valve for obstruction management
R1	Calibrated orifice
O_2S	Oxygen sensor

2.1.2 Ventilation Operation

The ventilator's turbine (T) draws ambient air through the Monnal Clean'In filter (HEPA) (H2), ensuring sufficient compression based on the patient's needs and set parameters. The compressed gas is then distributed through the pneumatic circuit (Figure 2.2), depending on whether the system is in the inspiratory or expiratory phase.

2.1.2.1 Inspiratory Phase

During the inspiratory phase, the turbine (T) regulates:

- Flow, via the flow sensor (FS1) in volume control mode.
- Pressure, via the pressure sensor (PS1) in pressure control mode.

Simultaneously, solenoid valve V3 is open, and V2 is closed, allowing turbine pressure to act on the expiratory valve membrane, ensuring that airflow is directed toward the patient.

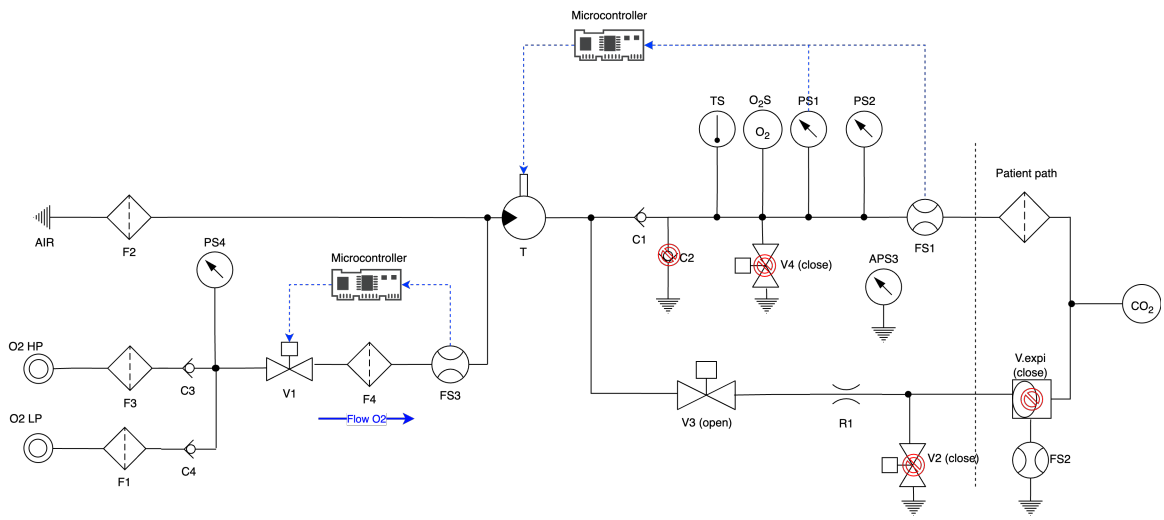

Fig. 2.3: Pneumatic diagram during the inspiratory phase

2.1.2.2 Expiratory Phase

During expiration, the patient exhales previously inhaled gases, and the system regulates positive end-expiratory pressure (PEEP) according to the set parameters.

To achieve this:

- The proportional solenoid valve (V2) modulates expiratory pressure based on feedback from the pressure sensor (PS1).
- The turbine (T) maintains a Flowby level of 5 L/min, regulated by the flow sensor (FS1).

This controlled expiratory flow prevents re-inhalation and ensures rapid detection of inspiratory effort, facilitating trigger detection.

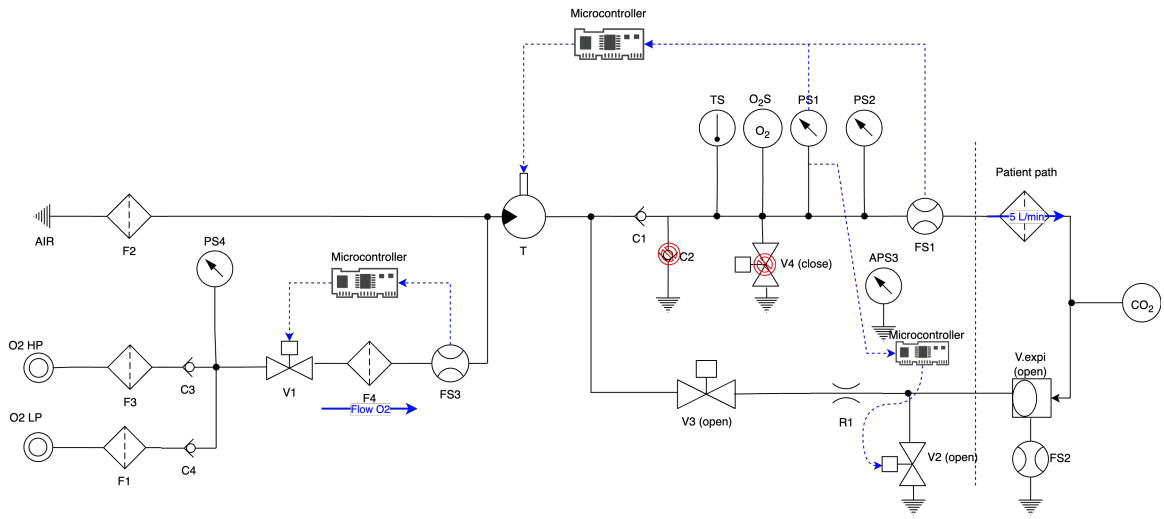

Fig. 2.4: Pneumatic diagram during the expiratory phase

2.1.3 Control Strategies Based on Ventilation Mode

The regulation strategy varies depending on the selected ventilation mode:

2.1.3.1 Pressure Control Ventilation (PCV)

In PCV mode, the system targets a pressure setpoint P_i using a two-stage PI (Proportional-Integral) controller. Since the pressure sensor (PS1) is located at the turbine outlet, the control does not directly compensate for pressure losses induced by the patient's respiratory system (lungs + circuit compliance and resistance).

To address this limitation:

- The setpoint pressure is adjusted to 107% of the target pressure (with an allowable overshoot up to 110%) to compensate for circuit losses.

The two PI controllers operate as follows:

1. *Rise phase:* The first PI controller is tuned for a fast rise time, ensuring rapid pressure buildup.
2. *Plateau phase:* Once the target plateau pressure is reached, the system switches to a less aggressive PI controller to eliminate steady-state error while maintaining stability.

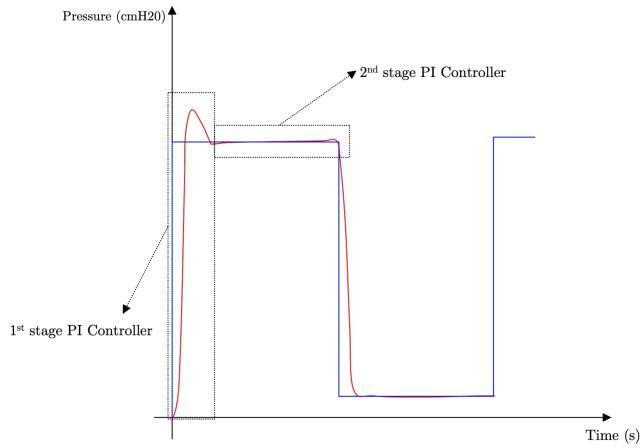

Fig. 2.5: Two Stage PI Controller

2.1.3.2 Volume Control Ventilation (VCV)

In VCV mode, a similar two-stage PI control strategy is applied:

- The first PI controller ensures rapid flow ramp-up.
- The second PI controller maintains the target flow rate throughout the inspiratory phase.

However, unlike in PCV, adaptive PI tuning is implemented:

- *Rise phase adaptation*: During this phase, the coefficients K_i and K_p are dynamically adjusted based on the patient category and target flow rate. For instance, if the overshoot is below 5%, the K_i coefficient is increased to improve response time.
- *Constant flow phase adaptation*: The proportional (K_p) and integral (K_i) gains are adjusted in real time based on oscillation detection.

2.2 Pressure and flow regulation strategy in pulmonary ventilators

In an industrial context, it is often difficult to find articles that explicitly describe pressure and flow regulation strategies in pulmonary ventilators.

In [6], the authors develop a control method that enables precise tracking of a time-varying target pressure while accounting for unknown parameters such as the patient, the hose, leaks, and the patient's breathing effort. This approach relies on an online estimation of the hose characteristics to dynamically compensate for the pressure drop it induces.

To achieve an output pressure $p_{\text{out}} = p_{\text{control}}$, an accurate lookup table is used in conjunction with a feedback controller based on the error $p_{\text{control}} - p_{\text{out}}$. This lookup table determines the required blower RPM to achieve the desired outlet pressure p_{out}, given the measured outlet flow Q_{out}. The feedback controller then eliminates the remaining blower error. However, to compensate for the pressure losses caused by the hose, the authors introduce an *adaptive controller* that dynamically adjusts the control command by estimating the hose's linear resistance, R_{lin}, in real time.

The estimation of R_{lin} is performed online based on the measured flow rate Q_{out} to compensate for the pressure drop:

$$\hat{p} = R_{\text{lin}} Q_{\text{out}}$$

The control pressure is then dynamically adjusted as follows:

$$p_{\text{control}} = p_{\text{target}} + \hat{p}$$

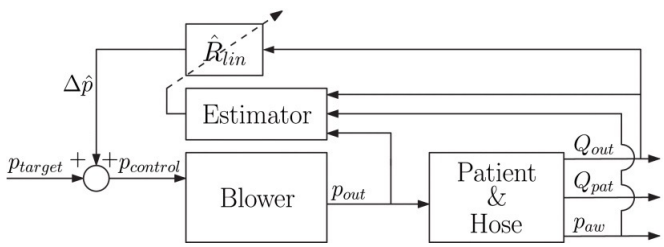

Fig. 2.6: Schematic of the proposed closed-loop system with an RLS estimator for the hose resistance estimation [6].

Thus, the ventilator directly generates the necessary pressure to compensate for the losses in the hose, ensuring precise tracking of the target pressure.

In [4], the authors develop a control method that enables precise tracking of a time-varying target pressure while ensuring stability and robustness against disturbances such as patient effort and system nonlinearities. This approach relies on the implementation of two control strategies: Proportional-Integral (PI) control and Linear Quadratic Regulator (LQR) control, both tested on a non-invasive mechanical ventilator.

To achieve an output volume or pressure that follows a given reference, the system employs a closed-loop control scheme where the ventilator motor's speed is adjusted in real-time based on measured feedback. The PI controller provides a simple yet effective correction by integrating the error between the desired and actual values, while the LQR controller optimally minimizes deviations using a quadratic cost function.

The PI control law is defined as:

$$u(t) = K_p e(t) + K_i \int_0^t e(\tau) d\tau$$

where K_p and K_i are the proportional and integral gains, respectively.

Alternatively, the LQR controller uses a state-space representation of the system to compute an optimal feedback gain matrix K based on Ricati equation:

$$A^T P + PA - PBR^{-1}B^T P + Q = 0$$

where P is a symmetric positive definite matrix. The optimal gain K is then obtained as:

$$K = R^{-1}B^T P$$

The resulting control law is:

$$u(t) = -Kx(t)$$

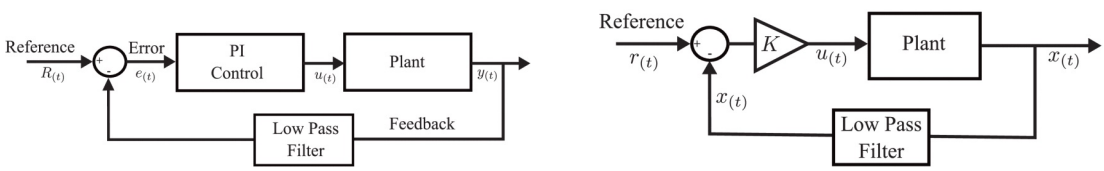

(a) PI controller (b) LQR Controller

Fig. 2.7: Block Diagram of controllers [4].

In figure 2.7, $r(t)$ are the desired volume and flow or the desired pressure, $y(t)$ is the mesured volume or the measured pressure and $u(t)$ is the PWM or the speed command sent to the motor driver.

Chapter 3

Technical choices and Description of achievements

3.1 Expiratory Phase Regulation

The regulation of positive End Expiratory Pressure (PEEP) and flushing flow (Flowby) in the pneumatic circuit represents a major challenge during the expiratory phase of the respiratory cycle.

The specifications require:

- A PEEP between 0 and 40 cmH_2O.
- A Flowby lower than 5 L/min.
- A turbine operating at low speed to minimize oxygen consumption.

The main challenge lies in the simultaneous control of three parameters (pressure, flow, and turbine speed) using only two actuators (the turbine and a solenoid valve).

During the expiratory phase, the expiratory valve opens to allow the patient to exhale. However, to maintain a pressure above atmospheric pressure, the valve must be precisely controlled to ensure PEEP and keep the pulmonary alveoli open.

Currently, these valves are pressure-controlled based on the following principle:

- Inspiratory phase: The control pressure equals the circuit pressure, keeping the valve closed by pressure balance.
- Expiratory phase: A pressure lower than that of the circuit is applied, partially or completely opening the valve to regulate expiration and PEEP.

However, several problems have been encountered with this control method:

- Slow response time: difficulty ventilating patients with high respiratory rates.
- Excessive expiratory braking: which may disrupt the respiratory cycle.

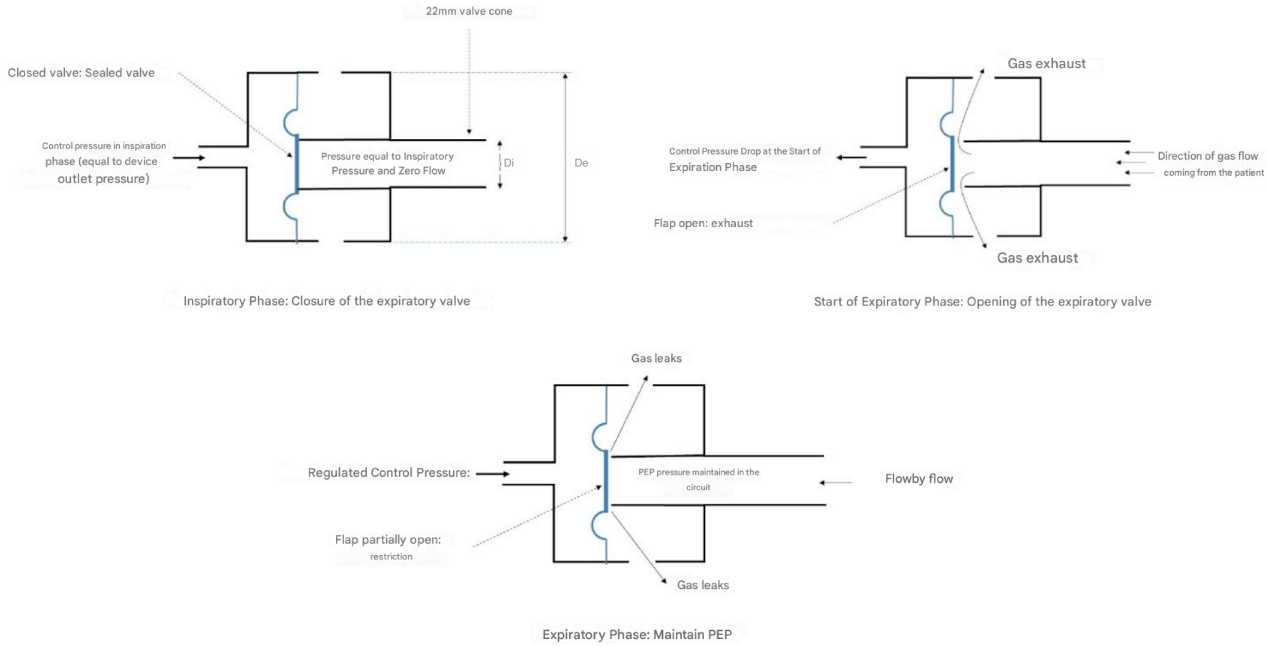

Fig. 3.1: Current diagram of the pressure-controlled valve during a respiratory cycle

- Instability for high PEEP values (>10 cmH_2O): regulation difficulties and vibrations disrupting the ventilator's operation.

To meet the specifications and overcome the identified limitations, adopting a new actuator is considered. Two options were evaluated: using a Voice Coil Actuator (VCA) for electromechanical valve control, studied by Lucas Defer, or a proportional solenoid valve (PSV) for pneumatic control, which is the focus of this section. The goal is also to define a strategy for regulating PEEP and Flowby.

3.1.1 Description of the Solenoid Valve

The selected solenoid valve is a normally closed (NC), current-controlled proportional solenoid valve with three ports and two positions (3/2), featuring a maximum control current of 61 mA.

Modes of Operation:

- At rest: Port 2 is connected to port 3.
- Under control (current < 61 mA): Port 2 is partially connected to ports 1 and 3, allowing modulation of expiratory pressure.

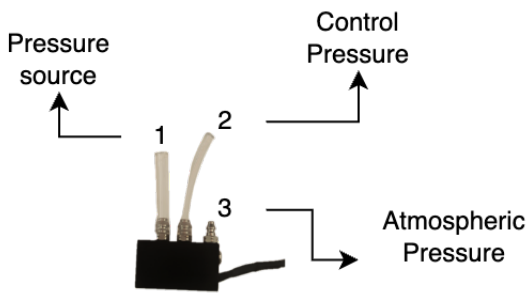

Fig. 3.2: (3/2) Proportional solenoid valve

3.1.2 Characterization of the Solenoid Valve

To ensure precise control of positive expiratory pressure (PEEP) and flushing flow (Flowby), an in-depth study of the proportional solenoid valve was conducted.

This characterization aims to:

- Determine the control current range of the solenoid valve based on the pressure in the expiratory branch.
- Analyze the dynamic response time to ensure fast and stable regulation.

The study was conducted on a test model reproducing the expiratory branch (Figure 2.2) of the Monnal T60 ventilator, allowing observation of the solenoid valve behavior under realistic conditions.

Two types of tests were performed:

1. *Static characterization*: Study the relationship between control current and output pressure of the solenoid valve.
2. *Dynamic characterization*: Evaluate the solenoid valve's response time for different PEEP levels.

These tests were performed for different turbine speeds (Table: 3.1) corresponding to the desired PEEP pressures at zero flow (expiratory valve closed).

3.1.2.1 Static Characterization

Methodology

Table 3.1: Tabulation of pressure at zero flow as a function of turbine speed

Turbine speed (rpm)	Zero flow pressure (mbar)
15 000	5
19 000	8
21 300	10
23 500	12
26 300	15
30 000	20
37 000	30
43 000	40
48 000	50
53 000	60
58 000	70

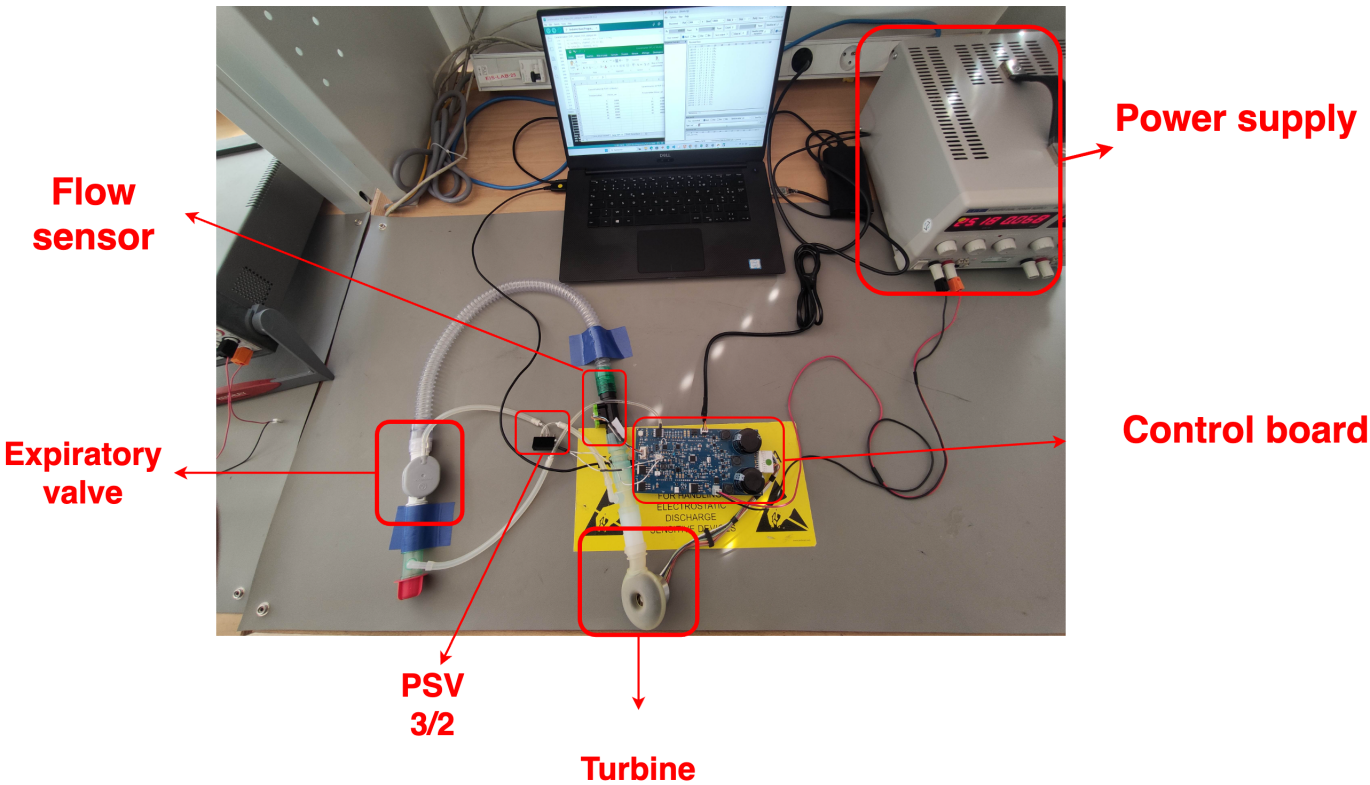

Fig. 3.3: Test bench for static and dynamic characterization

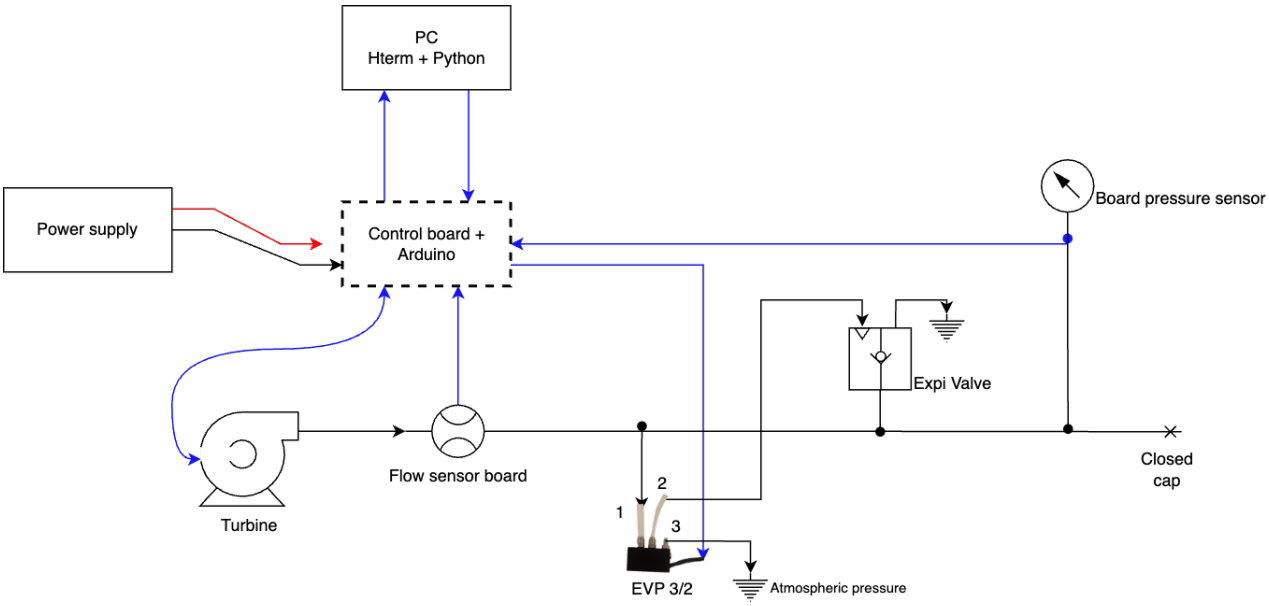

Fig. 3.4: Test bench block diagram

- The turbine is maintained at different speeds corresponding to the PEEP levels to be regulated (Table 3.1).
- An increasing and decreasing ramp between $I_{\min} = 1mA$ and $I_{\max} = 58mA$. is applied to the solenoid valve control.
- The output pressure is measured as a function of the control current.
- Special attention is paid to the decreasing pressure phase, corresponding to the patient's expiration.

3.1.2.2 Dynamic Characterization

Methodology

- The turbine is configured to generate different PEEP pressures at zero flow.
- The solenoid valve control current is abruptly switched between $I_{\min} = 1mA$ and $I_{\max} = 58mA$.
- The response time is measured for different configurations. It is defined as the sum of the delay and the rise time, where the rise time is the interval during which the pressure increases from 10% to 90% of its final value.

3.1.3 Implemented Regulation Strategy

Based on the dynamic and static characterization of the solenoid valve, which provided a maximum response time of 100 ms for regulating the highest PEEP levels and an effective control current range between 25 and 43 mA, we implement the PEEP and Flowby regulation strategy following the protocol below.

The real-time measurements used for regulation are:

- *Proximal pressure*: Pressure at the patient level, measured via a manometer integrated into the control board.
- *Inspiratory flow*: Measured by a flow meter.
- *Turbine speed*: Measured using a Hall effect sensor.
- *PSV control current*: Dynamically adjusted via a PI controller.

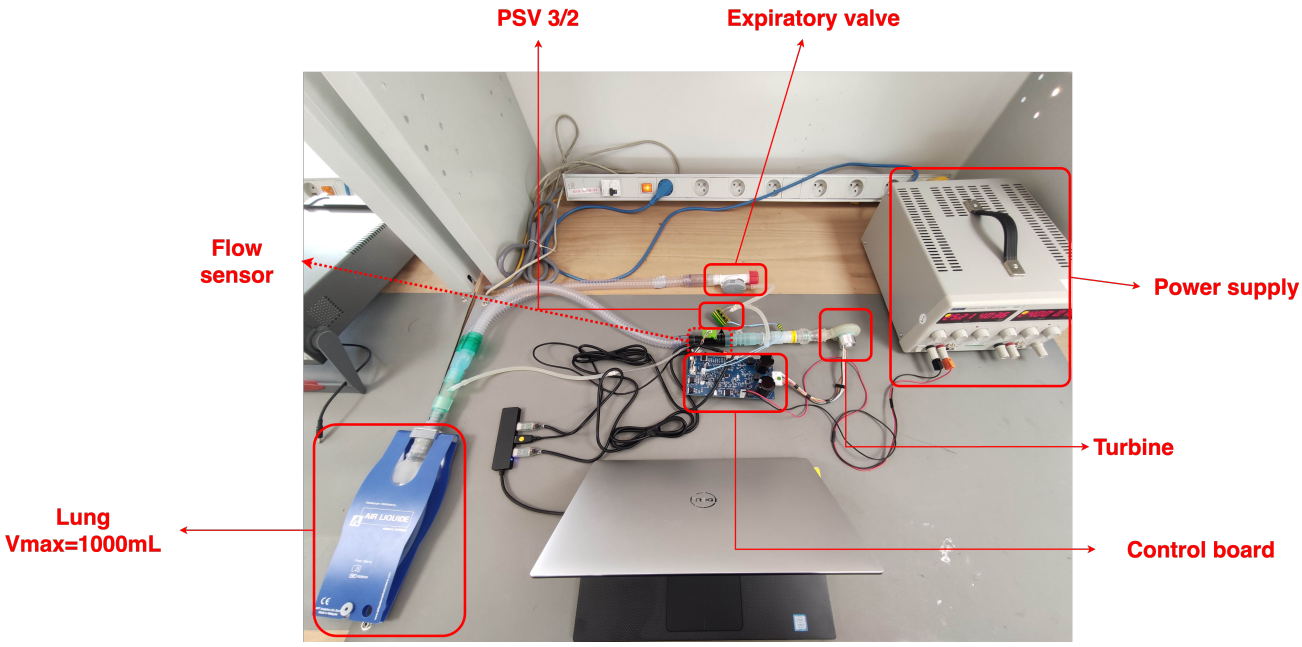

Fig. 3.5: Test bench for PEEP regulation

1. *Inspiratory Phase Regulation*

   During the inspiratory phase, a volumetric or barometric PI regulation is applied to the turbine to deliver a specific inspiratory volume or pressure. The expiratory valve is completely closed, and the PSV is activated with a control current corresponding to $\frac{3}{4}$ of the maximum current.

2. *Expiratory Phase Regulation*

   The expiratory phase is divided into two sub-phases:

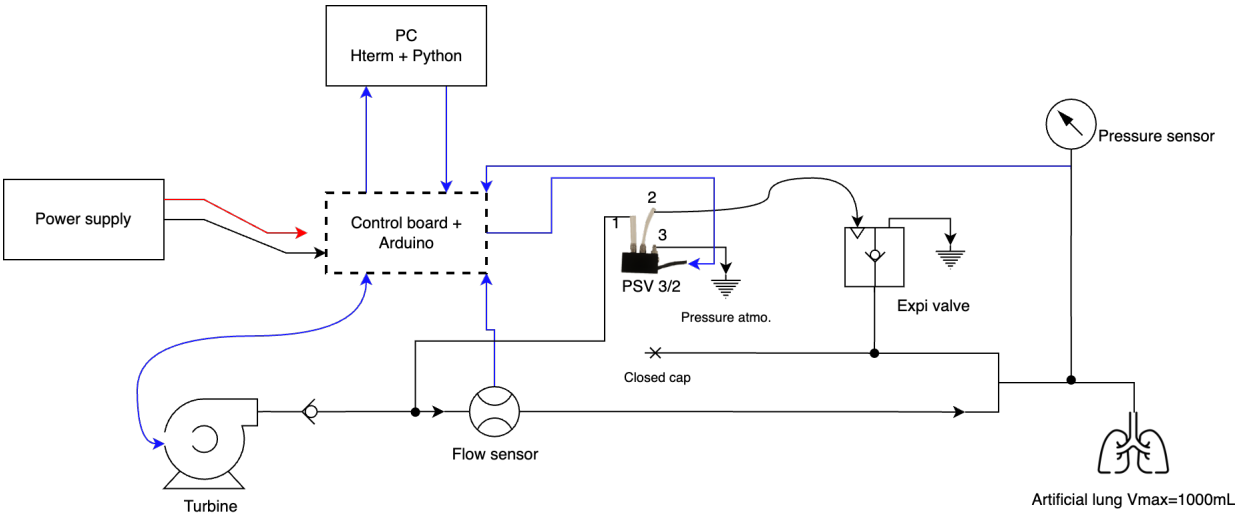

Fig. 3.6: Test bench block diagram for PEEP regulation

Braking Phase During this phase, the turbine is slowed down to achieve the fastest possible descent slope. To do this, a PWM signal corresponding to 10% of the maximum control signal is sent. This phase ends when the turbine speed becomes lower than the speed necessary to reach the proximal pressure corresponding to the desired PEEP or when the braking time exceeds 100 ms.

The expiratory valve is fully open to allow gas expiration, with the solenoid valve controlled at a minimum current of 20 mA.

PEEP Stabilization Phase After the braking phase, PEEP regulation begins:

- A turbine speed PI regulation is applied to maintain a speed corresponding to the proximal pressure at zero flow.
- A PI regulation of the PSV control current is implemented to ensure a given PEEP.

Key considerations:

- PI saturation values were set to $I_{\text{MIN_Cmd}} = 37.6$ mA and $I_{\text{MAX_Cmd}} = 42.0$ mA, determined through successive tests.
- PI coefficients are adjusted for a fast system, even if it causes slight oscillations, which remain within a consistent range.
- PI equation coefficients are initialized during the braking phase.

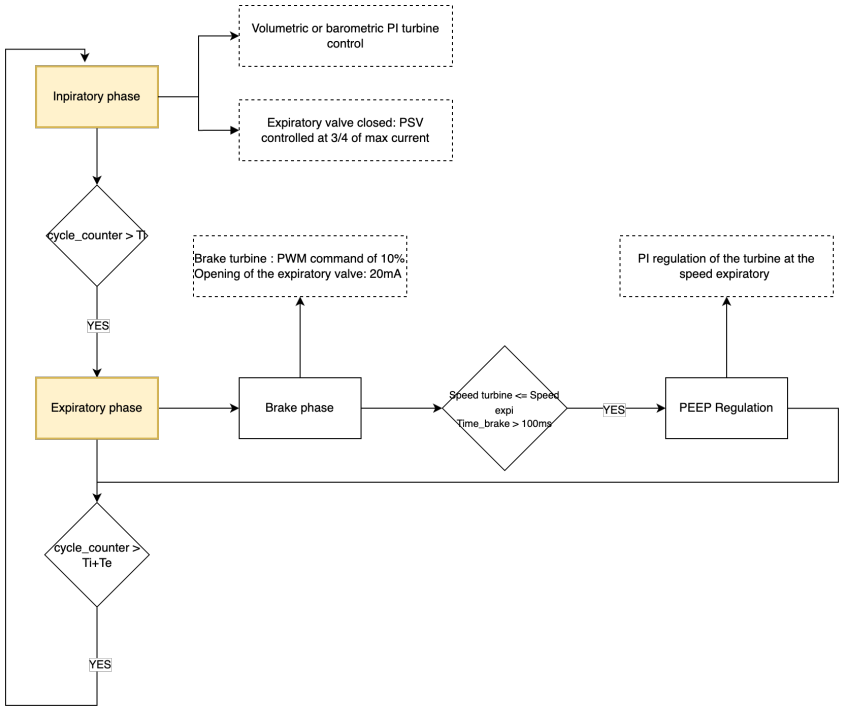

Fig. 3.7: Flux diagram of expiratory phase strategy

3.2 Inspiratory Phase Regulation

The regulation of pressure or flow is a major challenge for a ventilator, particularly during the inspiratory phase. The key component of the ventilator, the turbine, must be precisely controlled to ensure proper pressure or flow regulation. In practice, this involves mastering the turbine speed. The primary objective is to ensure effective ventilation that meets the requirements outlined in the specifications (1.3) for different patient categories.

The initial strategy for pressure and flow regulation involved decoupling high-level pressure/flow control from turbine speed control. In other words, a regulation strategy was implemented to satisfy the specification requirements, generating corresponding turbine speed profiles. The objective was then to implement a low-level turbine control to follow these speed profiles. However, this strategy proved ineffective due to the dual regulation process, which introduced significant delays. This led us to explore alternative approaches for direct high-level pressure/flow regulation.

An important aspect of regulation in this phase is determining the appropriate frequency for turbine control. Since the turbine is the primary actuator in this phase, its response to a step PWM command was analyzed (Figure 3.8). Precision measurements provided the following characteristics (Table 3.2):

By selecting a resolution of 10 points during the turbine's transient phase, we set $T = 10 * T_s$, which gives $T_s = 10ms$. Thus, we choose $T_s = 10$ ms, resulting in

Table 3.2: Time characteristics of the open-loop speed response

Delay time (L)	Rise time (T)	Gain (Speed/PWM)
8 ms	100 ms	12.96

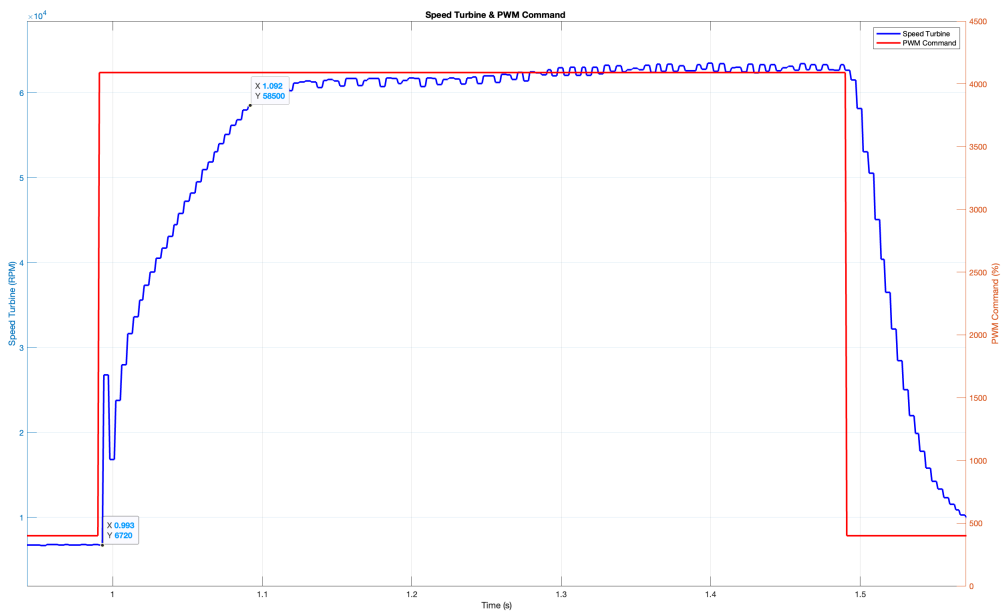

Fig. 3.8: Open-loop response of Speed to a PWM command of 4050

a regulation frequency of 100 Hz.

To achieve these regulation objectives, signal preprocessing was performed to identify the most suitable filter that minimizes noise while introducing the least possible delay.

3.2.1 Signal Processing: Signal Filtering

The flow and pressure sensor signals are sampled at 1 kHz and filtered using a 10-sample moving average filter. This filter, with a constant coefficient of 1/10, serves as a low-pass filter that smooths the data while effectively reducing the sampling rate to 100 Hz, aligning it with the control frequency. Additionally, it has a low computational cost. However, Bode diagram analysis reveals a cutoff frequency of 44 Hz with an attenuation of -3 dB (Figure 3.9), which is insufficient for noise suppression. High-frequency noise, likely induced by pneumatic system vibrations, remains particularly problematic during volume-controlled ventilation (Figure 3.10). To address this, alternative filtering approaches were explored, including a decimation filter and a combination of a 1 kHz Butterworth low-pass filter followed by a 10-sample moving average filter.

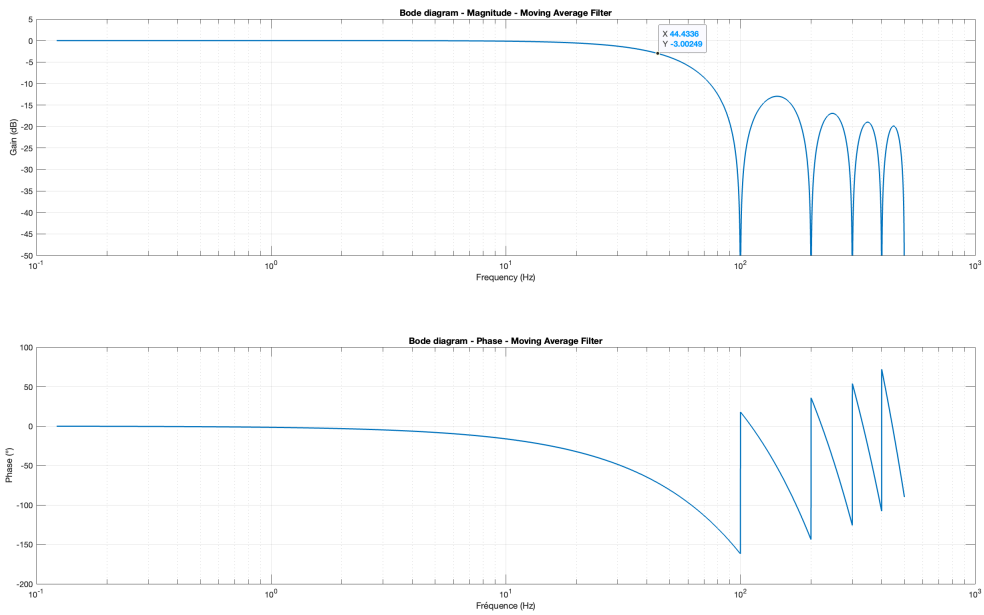

Fig. 3.9: Bode diagram of the N=10 window moving average filter, Fs = 1Khz

These approaches were initially tested for a ventilation frequency of 20 breaths per minute (bpm), corresponding to a common ventilation rate. The filter behavior was then analyzed for higher frequencies, allowing for parameter adjustments based on the obtained results. Before detailing the tests, it is important to recall the

main objective of filtering: eliminating high-frequency components from pneumatic noise while preserving fundamental signals related to the ventilation frequency (Fr) and signal components containing 90% ± (5%) of the total energy. The goal is to minimize the distortion introduced by the filter.

To achieve this, the flow spectrum (Fourier Transform) was analyzed, along with the spectral density to evaluate the energy associated with each frequency. This analysis identified the harmonic multiple of the ventilation frequency (Fr) beyond which 90%±(5%) of the total signal energy is contained. In this case, it corresponds to 9Fr for ventilation at 20 bpm.

3.2.1.1 Test Protocol Description

Signals are acquired in open-loop mode at a frequency of 1 kHz. The turbine is controlled via PWM with a square wave signal and an inspiration/expiration (I/E) ratio of 1/2. In this configuration, the turbine speed is not regulated. The control generates a pressure of 40 mbar in the lung, from which the flow is derived, simulating respiratory cycles at a frequency of 20 bpm.

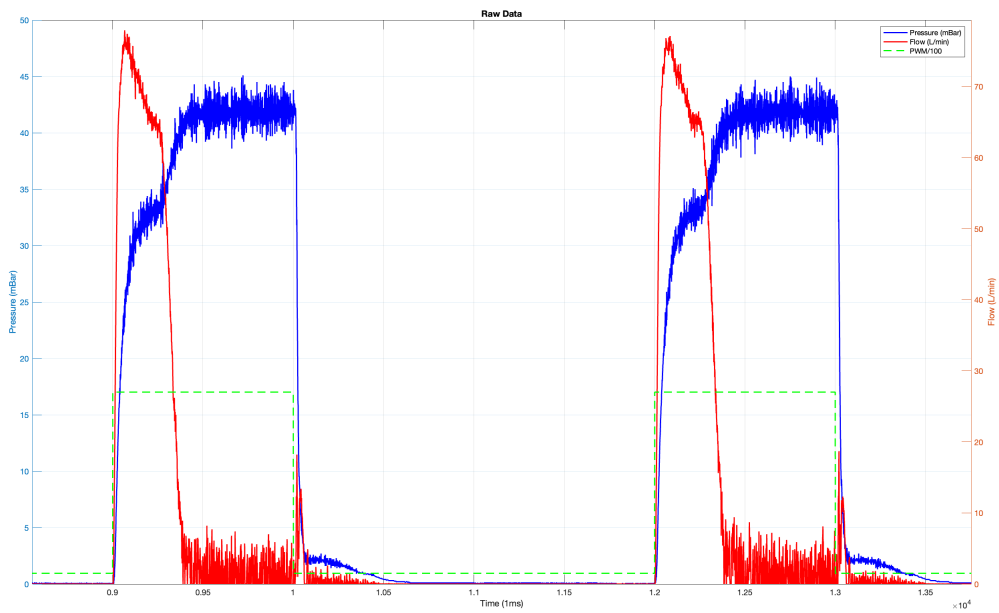

Fig. 3.10: Pressure and flow data over two ventilation cycles at 1 kHz. Blue: Pressure ; Red: Flow.

3.2.1.2 Decimation Filter

Decimation involves reducing a signal's sampling frequency by an integer factor, also known as "down-sampling." This process is accompanied by low-pass filtering to remove high-frequency components from the signal to meet the constraints of the new sampling frequency. A typical decimation filter, known as an M-fold filter, consists of two stages: - A FIR low-pass filter (anti-aliasing) H(z) to remove high frequencies. - A decimator that retains one sample out of M and discards the others.

The initial sampling frequency f_S is reduced by a factor of M, resulting in an output signal with a new sampling frequency of f_S/M. In this study, the `Signal Processing` toolbox of MATLAB was utilized, specifically the `decimate` function. This function applies an 8th-order Chebyshev Type I low-pass filter with a normalized cutoff frequency of $0.8/M$ and a passband ripple of 0.05 dB. For a decimation factor of $M = 10$, the cutoff frequency is calculated as follows:

$$f_c = \frac{0.8}{10} \times \left(\frac{1000}{2}\right) = 40 \text{ Hz}$$

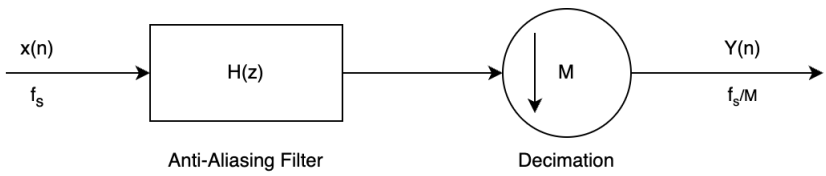

Fig. 3.11: Decimation Filter

3.2.1.3 Butterworth Filter + Moving Average over 10 Samples

The design of the Butterworth low-pass filter is based on a detailed spectral analysis of the signal, aiming to retain between 90% and 95% of the total energy while effectively eliminating high-frequency components. The goal is to design a filter that preserves this energy range while introducing the smallest possible delay, without significantly distorting the visual appearance of the signal.

1. *Signal Parameters*
   - *Fundamental frequency:* $F_R = \frac{1}{3}$ Hz, corresponding to a ventilation rate of 20 breaths per minute (bpm).
   - *Sampling frequency:* $f_s = 1000$ Hz.
2. *Fourier Transform (FFT)*

   The Fast Fourier Transform (FFT) converts the time-domain signal into its frequency spectrum, providing the amplitude of each frequency component.

Frequency resolution: The frequency associated with each sample is determined by the resolution Δf, calculated as:

$$\Delta f = \frac{f_s}{N}$$

where:

- f_s is the sampling frequency.
- N is the total number of samples.

The frequency corresponding to a given sample k is then:

$$f_k = k \cdot \Delta f$$

3. *Harmonic Identification*

   Harmonics are defined as integer multiples of the fundamental frequency: $F_R, 2F_R, 3F_R, \ldots, nF_R$. To identify harmonics in the spectrum:

   - The harmonic index k_{harmonic} corresponding to each harmonic nF_R is calculated as:

   $$k_{\text{harmonic}} = \frac{(n \cdot F_R)}{\Delta f} = \frac{(n \cdot F_R \cdot N)}{f_S}$$

   - This index allows the identification of the spectral amplitudes associated with each harmonic.

4. *Energy per Harmonic*

   The energy associated with each harmonic is determined from the squared magnitude of its amplitude in the frequency spectrum. Specifically:

   - The spectral contributions of nearby frequencies around each harmonic are summed.
   - The total energy around the harmonic nF_R is computed as:

   $$E_{\text{harmonic}} = \sum_{f \in \text{band around } nF_R} |X(f)|^2$$

   where $X(f)$ represents the complex amplitude at frequency f.

5. *Total and Cumulative Energy*

   The total energy of the signal is given by:

   $$E_{\text{total}} = \sum_{f \in \text{spectrum}} |X(f)|^2$$

   Cumulative energy analysis was performed to determine the number of harmonics required to retain 90% ($\pm$5%) of E_{total}.

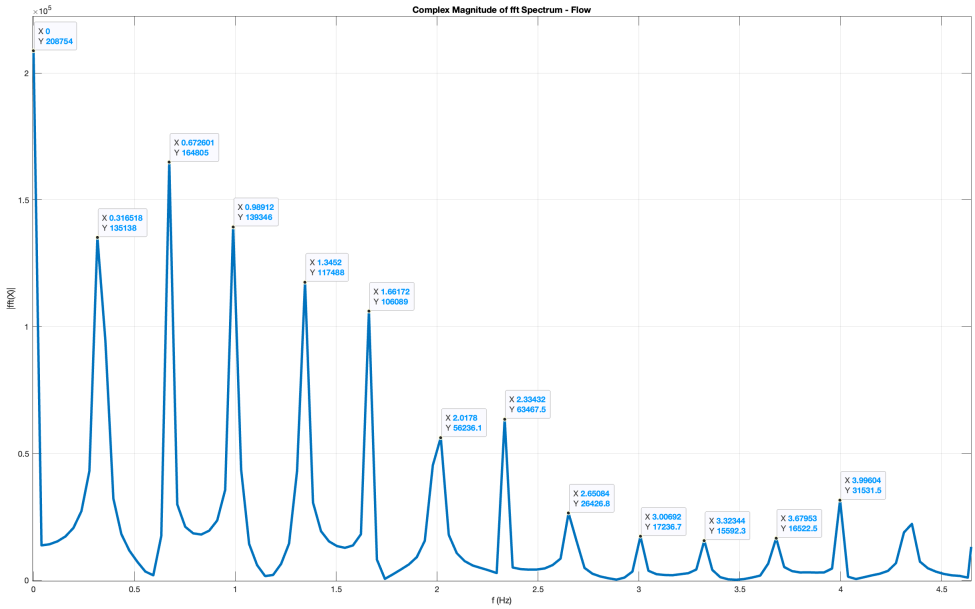

Fig. 3.12: Frequency spectrum

6. *Cutoff Frequency Determination*

   The analysis revealed that 90% (±5%) of the total signal energy is contained within the first nine harmonics (Figure 3.13), with a maximum harmonic order of:

$$n_{\max} = 9$$

   Chosen cutoff frequency:

$$f_c = n_{\max} \cdot F_R = 9 \times \frac{1}{3} = 3 \text{ Hz}$$

7. *Design Using MATLAB*

   To achieve effective filtering with minimal distortions, the following criteria were defined:

   - *Passband:* 3 dB attenuation at the cutoff frequency f_c.
   - *Stopband:* 20 dB attenuation at 20 Hz.

   These requirements were used to design a Butterworth low-pass filter:

   - The MATLAB function `buttord` was employed to determine the optimal filter parameters.
   - The resulting *second-order* Butterworth low-pass filter satisfies both the passband and stopband attenuation constraints.

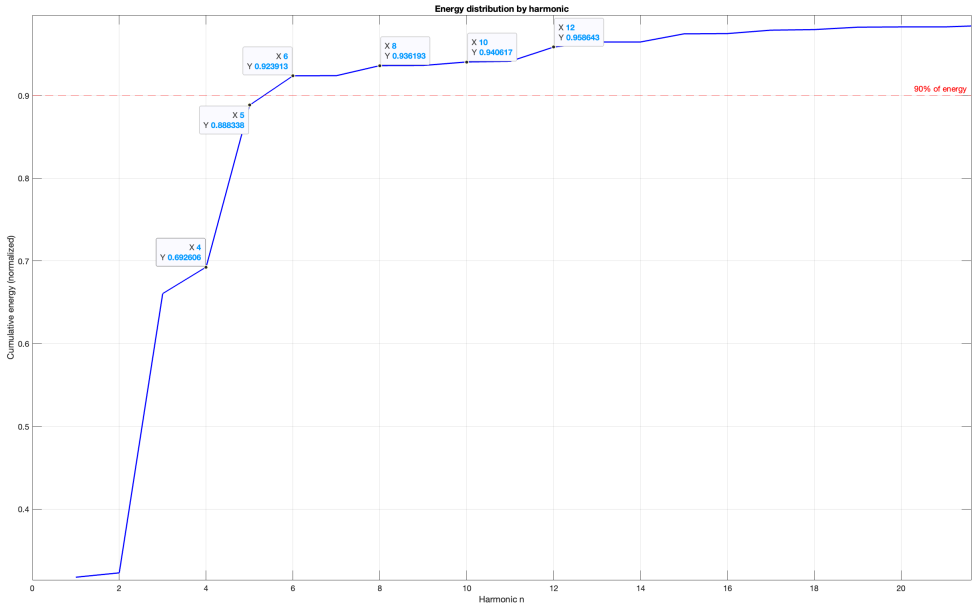

Fig. 3.13: Energy distribution by Harmonic

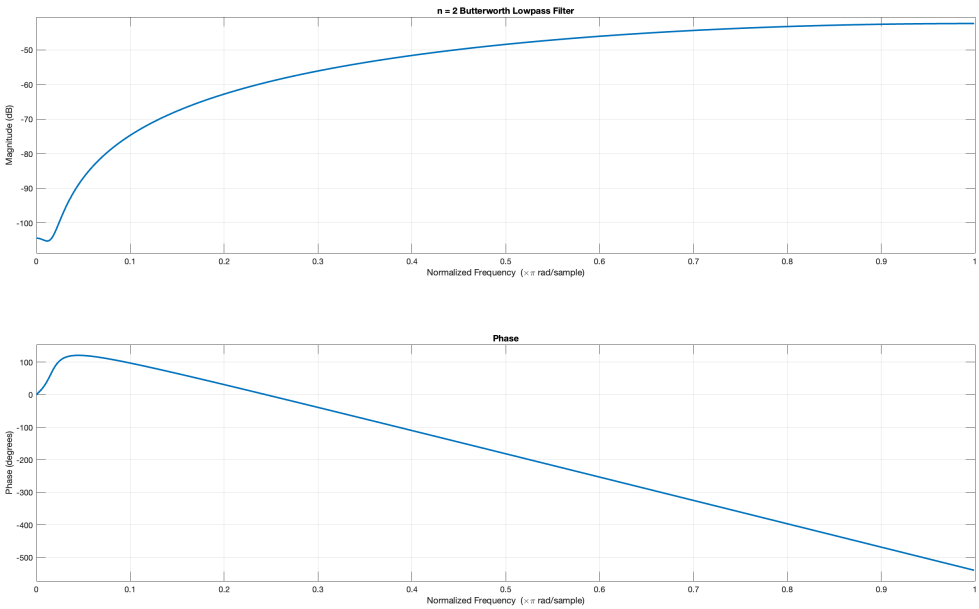

Fig. 3.14: Bode diagram of Butterwoth filter

3.2.2 Strategy 1: Decoupling of Pressure/Flow Control from Turbine Speed Control

The first control strategy involved decoupling high-level pressure/flow regulation from low-level turbine speed control.

A modeling of the pneumatic system and the turbine was coupled with the turbine's electrical model. Subsequently, pressure/flow regulation was performed using a PI controller configured for the rise phase and the plateau phase (2.1.3) to meet requirements for different patient categories. Compliance with the specifications was achieved. From this regulation, adequate pressure/flow profiles were obtained, along with corresponding turbine speed profiles. The objective was then to implement motor control to follow the various speed profiles, covering the entire spectrum of different patient categories.

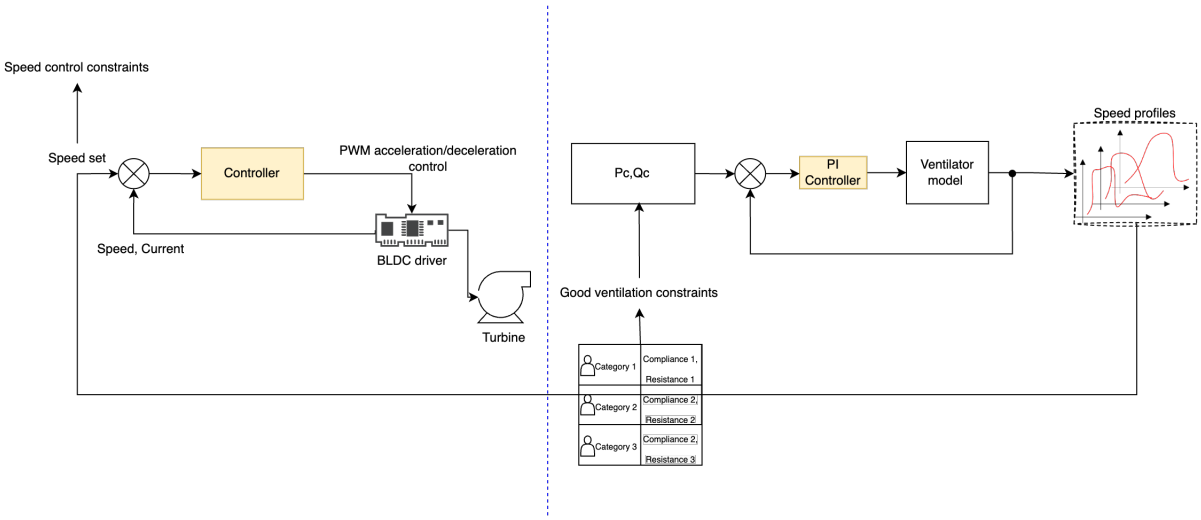

Fig. 3.15: Decoupling of Pressure/Flow Control from Turbine Speed Control

To achieve this, the modeling was conducted using Matlab Simulink. The two most important parts are the pneumatic and electrical sections of the turbine. The turbine characteristics provide the generated pressure as a function of speed and flow rate.

1. *Pneumatic Section*

   This section is modeled as a black box, derived from various tests conducted on the turbine.The model provides the generated pressure as a function of speed and flow rate (Figure 3.16).

2. *Electrical Section*

   The electrical part of the turbine was designed based on the equations of a DC motor. The block diagram modeling these equations is shown in Figure 3.17. The motor parameters are provided in Appendix B.

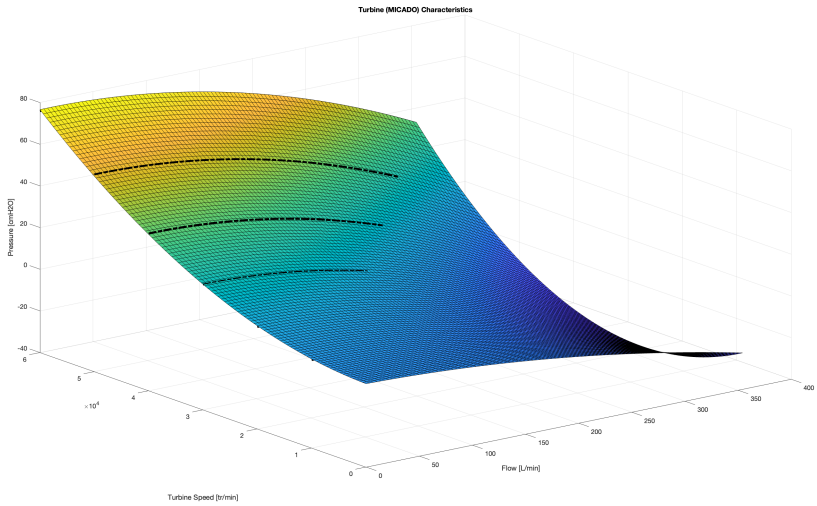

Fig. 3.16: Characteristics: Interpolated Speed, Pressure, and Flow for all speeds

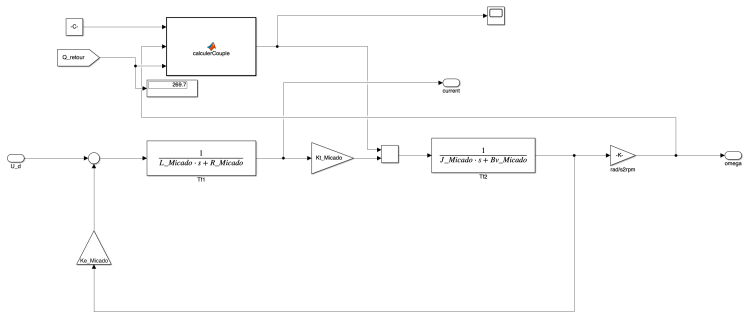

Fig. 3.17: Simulink model of the turbine's electrical section

Based on this model, the speed profiles were obtained from the first high-level regulation (Figure 3.18).

Two control approaches were used:

1. *Model Predictive Control (MPC)*

   Model Predictive Control is an advanced control method based on a precise mathematical model of the system, enabling the prediction of its future behavior. Thus, a state-space model of the system is required. Since the turbine control signal is a 12-bit PWM command (ranging from 0 to 4095) and the output is the turbine speed, system identification was performed using MATLAB's `System Identification` toolbox. Open-loop PWM step responses were recorded at 1 kHz (training and validation data) (Figure 3.19).

   To determine the system order, state-space models of order 1, 2, and 3 were tested. The model with the best fit on the validation data was a second-order state-space representation with a validation accuracy of 79.51%. The corresponding matrices are:

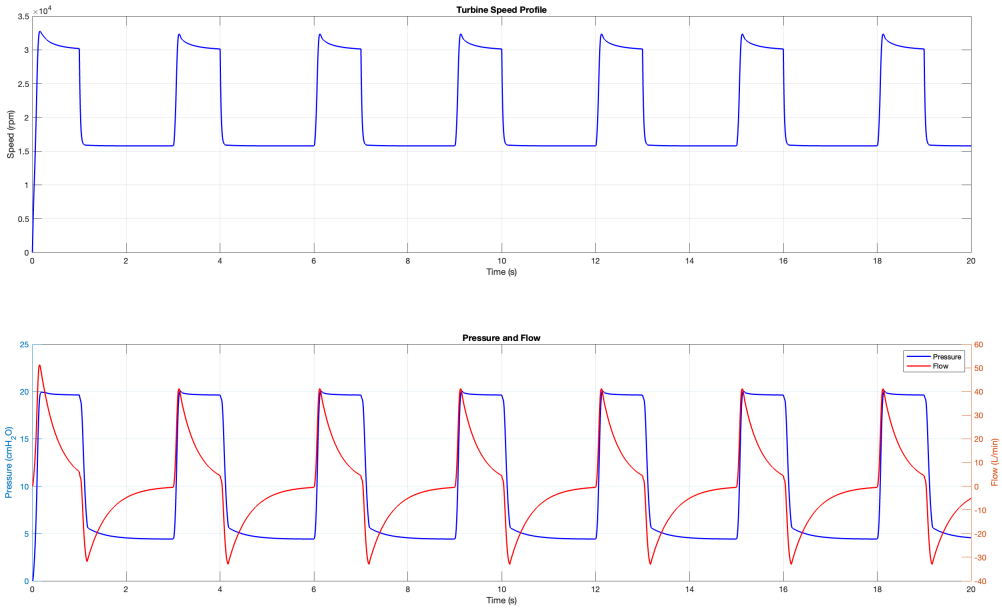

Fig. 3.18: Speed profile for a lung with compliance $C = 20\ L/cmH_2O$ and resistance $R = 20\ cmH_2O.s/L$ (R20C20), along with pressure and flow data.

$$A = \begin{bmatrix} 0.6384 & 0.2248 \\ 0.2500 & 0 \end{bmatrix}, \quad B = \begin{bmatrix} 4 \\ 0 \end{bmatrix}, \quad C = \begin{bmatrix} 0.7801 & 1.2491 \end{bmatrix}, \quad D = 1.1827$$

The MPC was implemented for a tracking problem (Appendix A) [5] with a prediction horizon of $N = 10$ and a control frequency of 100 Hz. The tracking problem involves finding the control sequence that minimizes the error between the reference and the system output over the prediction horizon. This is a quadratic optimization problem solved using MATLAB's `quadprog` function.

2. *PI Control*

   The PI controller is represented as:

$$U(z) = \frac{K_i T_s z}{z-1}\varepsilon(z) - K_p Y(z) \tag{3.1}$$

   with the discrete recursive equation:

$$u_k = u_{k-1} + K_i T_s (y_{c_k} - y_k) - K_p (y_{k-1} - y_k) \tag{3.2}$$

$$u_k = u_{k-1} + (K_i T_s - K_p) e_k - K_p e_{k-1} \tag{3.3}$$

   The Takahashi tuning method was used to determine K_p and K_i, which were then adjusted in closed-loop operation. From the turbine's speed response to

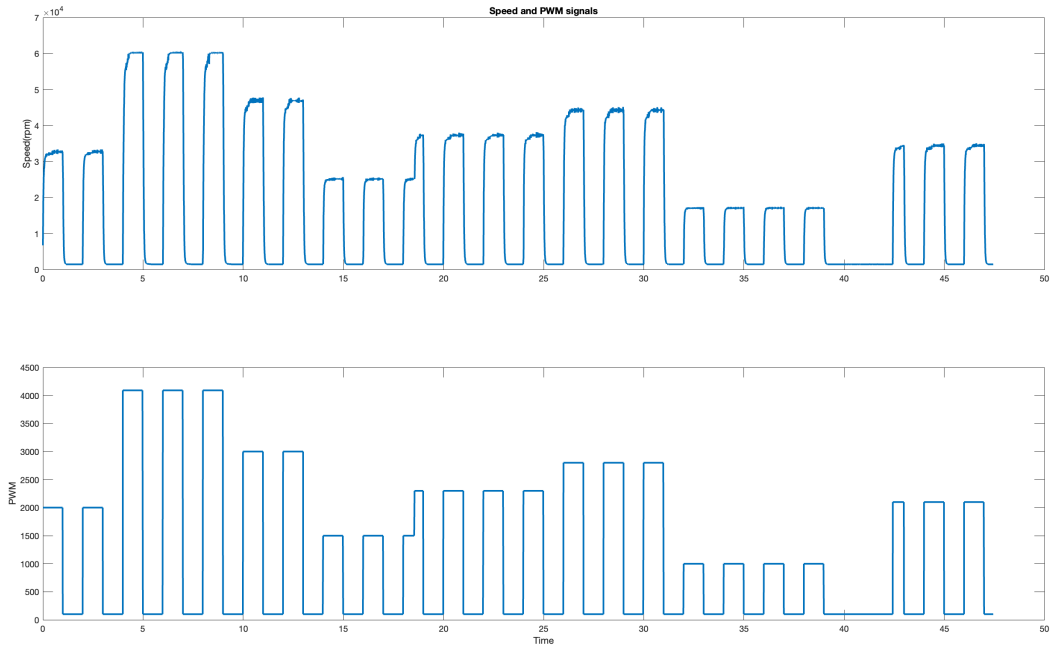

Fig. 3.19: Train data for turbine identification

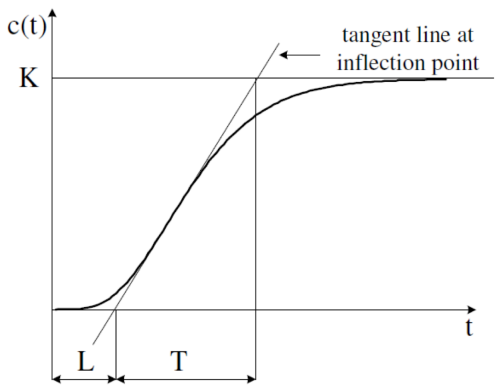

Fig. 3.20: Characteristics time for system identification

Table 3.3: Time characteristics of the open-loop speed response

Delay time (L)	Response time (T)	Slope $a = (K/T)$
8 ms	50 ms	12.96

a PWM step input (Figure 3.8), the characteristic times L and T (the time to reach 63% of the final value) were determined, as shown in Figure 3.20.

The PI gains are calculated as follows:

$$K_p = \frac{0.9}{a(L + 0.5T_s)} = 0.24, \quad K_i = \frac{0.27}{a(L + 0.5T_s)^2} = 6.38$$

The PI controller is implemented in the regulation loop as shown in Figure 3.21.

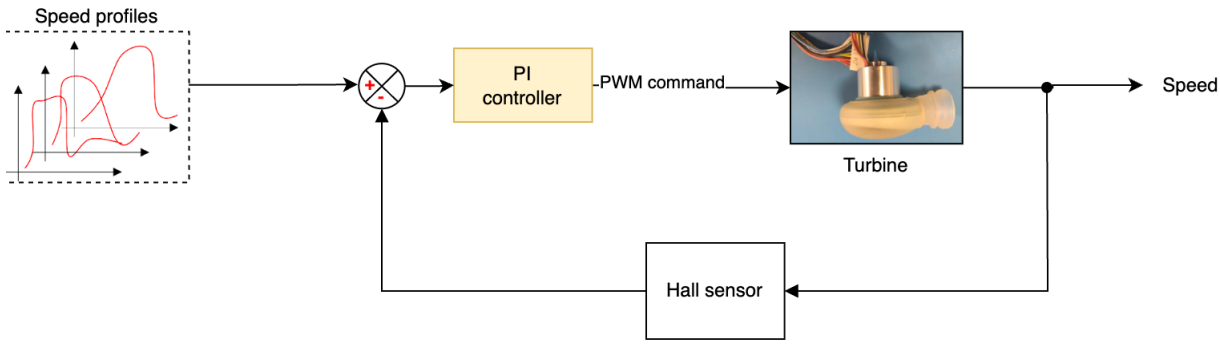

Fig. 3.21: Schematic of the PI Control Scheme

The real-time implementation of the PI controller was carried out on the Arduino Due board. The experimental protocol is identical to that of the PEEP regulation shown in Figure 3.6. However, the MPC could not be implemented in real-time due to its computational complexity, particularly the need to solve a quadratic optimization problem at each control period. Additionally, finding a robust C++ library for solving quadratic problems proved to be challenging.

3.2.3 Strategy 2: PI controller with cycle-by-cycle adaptation for pressure/flow rate

We implement a PI controller to regulate pressure and flow directly. The design process follows the same methodology as defined in the previous section for speed regulation, with the PI coefficients adjusted in closed-loop operation. In this case, we use the open-loop response of the proximal pressure (patient side) to a PWM step input, as shown in Figure 3.22.

In ventilation, it is acceptable for the pressure/flow to converge within five breathing cycles. Therefore, the control command is adjusted across cycles based on the errors observed in previous cycles, ensuring convergence within the required time frame.

The adaptation algorithm modifies the pressure/flow setpoint of the current cycle based on the error observed in the previous cycle. Specifically, at each control step k of cycle N, the setpoint is computed as:

$$r_{k,N} = r_{k,N-1} + \alpha e_{k,N-1}$$

where $e_{k,N-1}$ represents the error between the previous cycle's setpoint $r_{k,N-1}$ and the measured pressure/flow response $y_{k,N-1}$. The current error is then defined as:

$$e_{k,N} = r_{k,N} - \text{measure_pressure/flow}_{k,N}$$

The corresponding turbine control command is given by:

$$u_{k,N} = u_{k-1,N} + (K_i T_s - K_p) e_{k,N} - K_p e_{k-1,N}$$

where the PI gains are:

$$K_p = 2.2, \quad K_i = 470.$$

The factor α is determined in closed-loop operation, ensuring an appropriate trade-off to meet system requirements (1.3).

3.2.4 Strategy 3: Internal Model Controller

The Internal Model Control (IMC) philosophy is based on the Internal Model Principle, which states that effective control can be achieved only if the control system encapsulates, either implicitly or explicitly, some representation of the process to be controlled.

1. *IMC Strategy*

   In the diagram, $d(s)$ is an unknown disturbance affecting the system. The manipulated input $U(s)$ is introduced to both the process and its model. The

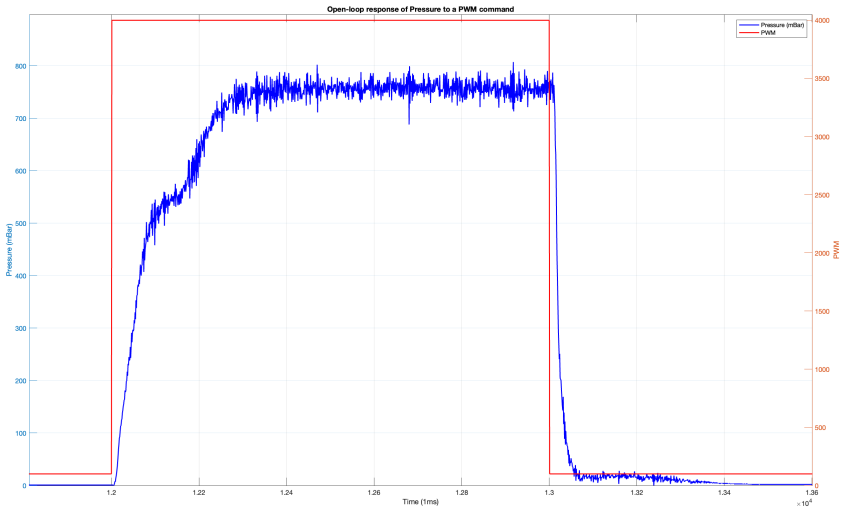

Fig. 3.22: Open-loop response of pressure to a PWM command.

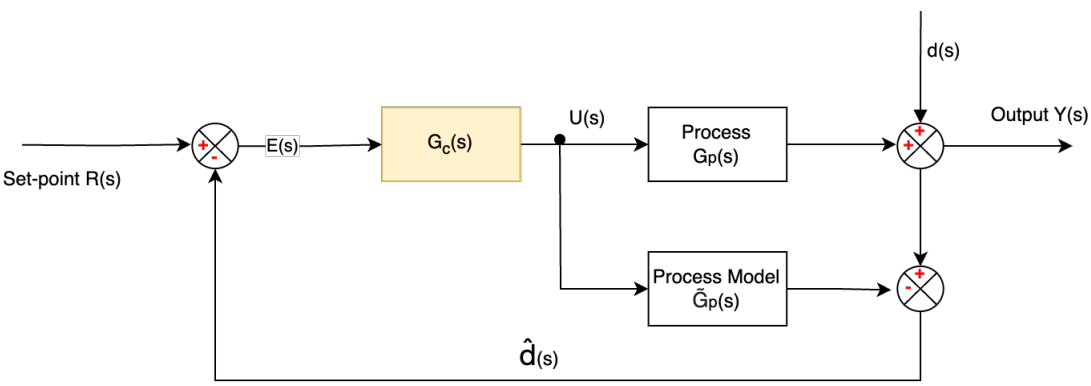

Fig. 3.23: Schematic of the IMC Scheme, inspired by [7]

process output, $Y(s)$, is compared with the output of the model, resulting in a signal $\hat{d}(s)$. That is,

$$\hat{d}(s) = \left[G_p(s) - \tilde{G}_p(s)\right] U(s) + d(s) \tag{3.4}$$

If $d(s)$ is zero, then $\hat{d}(s)$ measures the difference in behavior between the process and its model. If $G_p(s) = \tilde{G}_p(s)$, then $\hat{d}(s)$ equals the unknown disturbance.

Thus, $\hat{d}(s)$ may be regarded as the information missing in the model, $\tilde{G}_p(s)$, and can therefore be used to improve control. This is done by subtracting $\hat{d}(s)$ from the setpoint $R(s)$, which is similar to effecting a setpoint trim. The resulting control signal is given by:

$$U(s) = \left[R(s) - \hat{d}(s)\right] G_c(s) = \left\{R(s) - \left[G_p(s) - \tilde{G}_p(s)\right] U(s) - d(s)\right\} G_c(s) \tag{3.5}$$

Thus,

$$U(s) = \frac{[R(s) - d(s)]\, G_c(s)}{1 + \left[G_p(s) - \tilde{G}_p(s)\right] G_c(s)} \tag{3.6}$$

Since

$$Y(s) = G_p(s)U(s) + d(s) \tag{3.7}$$

the closed-loop transfer function for the IMC scheme is therefore:

$$Y(s) = \frac{G_c(s)G_p(s)R(s) + \left[1 - G_c(s)\tilde{G}_p(s)\right] d(s)}{1 + \left[G_p(s) - \tilde{G}_p(s)\right] G_c(s)} \tag{3.8}$$

From this closed-loop expression, we see that if $G_c(s) = \tilde{G}_p(s)^{-1}$ and $G_p(s) = \tilde{G}_p(s)$, then perfect setpoint tracking and disturbance rejection is achieved. Notice that, theoretically, even if $G_p(s) \neq \tilde{G}_p(s)$, perfect disturbance rejection can still be realized provided $G_c(s) = \tilde{G}_p(s)^{-1}$.

To enhance robustness, minimizing process-model mismatch effects is crucial. Since discrepancies between the process and its model typically occur at high frequencies, a low-pass filter $G_f(s)$ is introduced to mitigate these effects. Consequently, the internal model controller is designed as the inverse of the process model combined with a low-pass filter, formulated as:

$$G_{IMC}(s) = G_c(s)G_f(s)$$

The filter's order is selected to ensure stability and proper attenuation.

2. *IMC Implemenetation*

   We implement Internal Model Control (IMC) for pressure and flow regulation following our previous strategy. However, since we lack a clear transfer function for our system (turbine + pneumatic system), we rely on the empirical relationship between pressure, flow rate, and speed.

   Given a target pressure or flow rate and a current pressure or flow rate, we determine the required turbine speed. Conversely, for a given turbine speed and a specific pressure or flow rate, we obtain the corresponding output pressure or flow rate.

   In the IMC framework, our process takes a PWM command as input and outputs a pressure or flow rate. The model of this process is derived from the inverse of the previously established characterization (**??**). To ensure that the output follows the reference, the controller is defined as the inverse of the process model, meaning that it takes a pressure or flow rate as input and outputs the corresponding PWM command.

   From the previously established fan model, we have:

$$P = \left(a_1 Q^2 + b_1 Q + c_1\right)\Omega^2 + \left(a_2 Q^2 + b_2 Q + c_2\right)\Omega + \left(a_3 Q^2 + b_3 Q\right)$$

   where the coefficients are given as:

$$\begin{aligned} a_1 &= 1.63 \times 10^{-13}, & a_2 &= -1.33 \times 10^{-8}, & a_3 &= -1.52 \times 10^{-4}, \\ b_1 &= -5.82 \times 10^{-13}, & b_2 &= 2.99 \times 10^{-7}, & b_3 &= -9.96 \times 10^{-3}, \\ c_1 &= 2.01 \times 10^{-8}, & c_2 &= 7.23 \times 10^{-5}. \end{aligned}$$

   where Q is the flow rate in L/min and Ω is the turbine speed in rpm. This equation represents our process model. The controller is obtained by inverting this model as follows:

$$A\Omega^2 + B\Omega + C = 0$$

   where:

$$\begin{aligned} A &= a_1 Q^2 + b_1 Q + c_1, \\ B &= a_2 Q^2 + b_2 Q + c_2, \\ C &= a_3 Q^2 + b_3 Q - P. \end{aligned}$$

   The discriminant is computed as:

$$\Delta = B^2 - 4AC.$$

   The possible solutions for Ω are:

$$\Omega_1 = \frac{-B + \sqrt{\Delta}}{2A},$$
$$\Omega_2 = \frac{-B - \sqrt{\Delta}}{2A}.$$

Selection of the Physically Valid Solution:

- If the discriminant is negative ($\Delta < 0$), no real solution exists.
- If both solutions are valid ($\Omega_1 \geq 0$ and $\Omega_2 \geq 0$), the most appropriate solution for the application is chosen.

Special Case:

- If $A = 0$ (resulting in a linear equation), then:

$$\Omega = -\frac{C}{B}.$$

- If $B = 0$ as well, no unique solution exists.

Thus, the controller is obtained as $\Omega = f(P, Q)$. However, since the controller's output is a PWM signal, we need the relationship between turbine speed and PWM command.

To establish this relationship, characterization experiments were conducted under different configurations (zero flow, maximum flow, and varying flow). The relationship between turbine speed and PWM command was found to be quadratic:

$$\text{PWM} = 2 \times 10^{-7} \cdot \Omega^2 + 0.0544 \cdot \Omega + 87.051$$

with $R^2 = 0.9995$.

By combining these two models, we derive a controller that computes the corresponding PWM command based on the pressure error e.

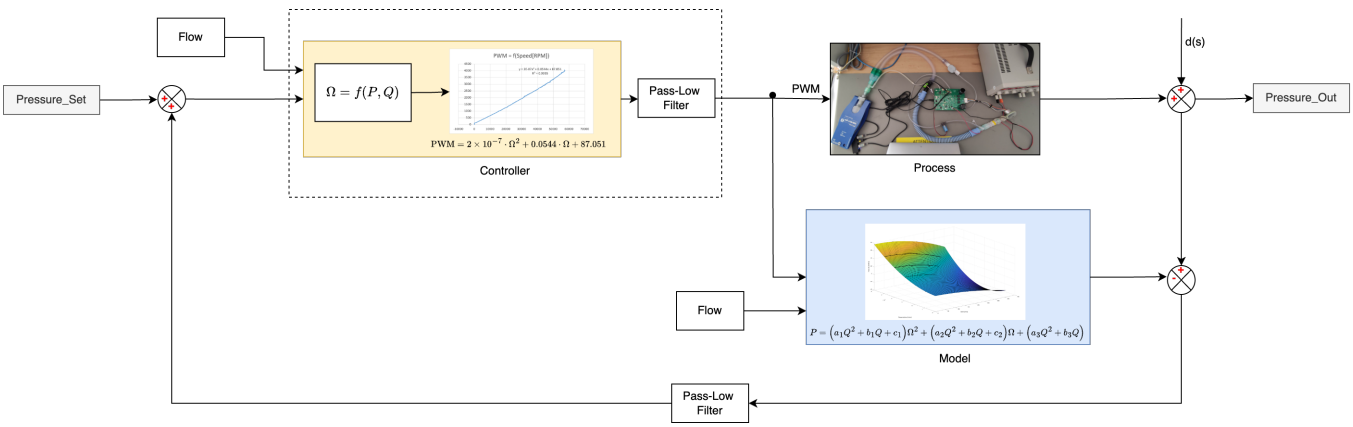

Fig. 3.24: Schematic of the IMC Implementation

Chapter 4

Results and Discussion

4.1 Signal Processing

Following the design of the two filters (decimation and Butterworth), we filtered the signals and compared them with the noisy signals, as well as with a 10-point moving average filter. Additionally, the Butterworth filter was tested at higher ventilation frequencies (60 and 100 bpm) to adjust the parameters accordingly.

4.1.1 Decimation Filter

Spectral analysis of the filtered signals shows that high-frequency components above 40 Hz are attenuated, although noise remains present below this threshold. The attenuation beyond 40 Hz is measured at 20 dB (Figure 4.1). Finally, a comparison with the 10-point moving average filter reveals minimal differences between the two methods.

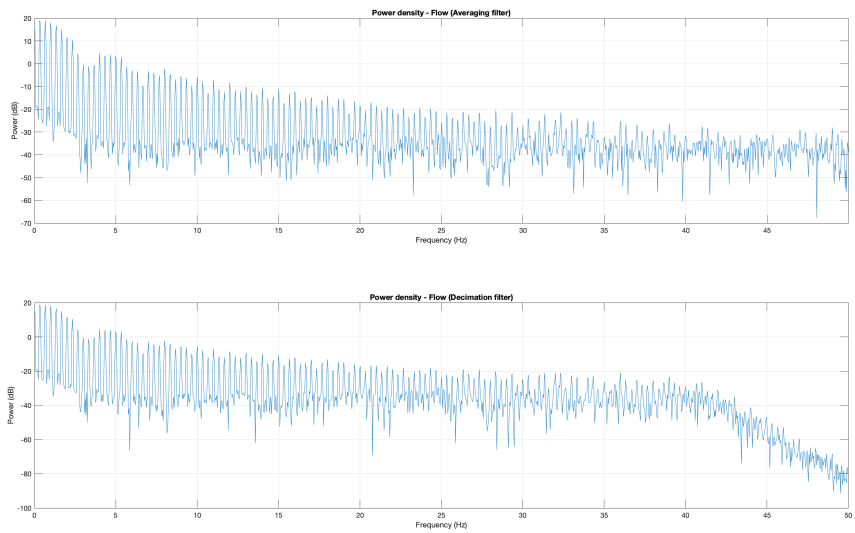

Fig. 4.1: Power spectral density of flow: Moving average filter vs. Decimation filter

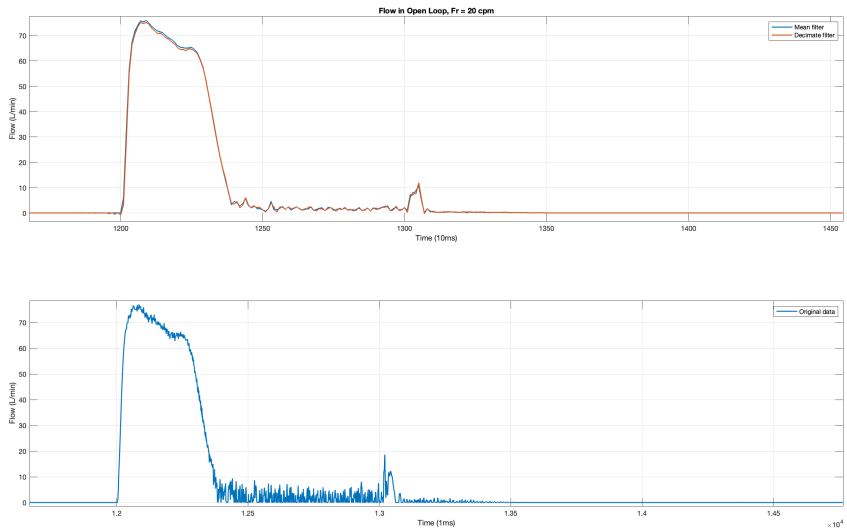

Fig. 4.2: Filtered flow sampled at 100 Hz and original flow at 1 kHz (Top: Blue - Moving average filter; Orange - Decimation filter)

4.1.2 Second-Order Butterworth Filter + 10-Point Moving Average

1. *Phase Shift*

   Comparing the filtered signal to the original, a delay of 50 ms is observed. This phase shift is inherent to the Butterworth filter characteristics. After initial filtering, a 10-point moving average filter was applied to further reduce noise and resample the data at 100 Hz (Figure 4.3).

2. *Power Spectral Density Analysis*

   The power spectral density analysis shows significant noise attenuation beyond the cutoff frequency f_c. However, slight signal distortion and phase shift are also observed (Figure 4.4).

3. *Signal Distortion Evaluation*

   To quantify the impact of distortion on the inspired air volume (corresponding to the area under the flow curve during inspiration), integration was performed using the trapezoidal method (Figure 4.5):

   - *Computed volume:* The area under the filtered flow curve was compared to the original signal.
   - *Relative error:* A negligible difference was observed, with a relative error of only 0.0155%.

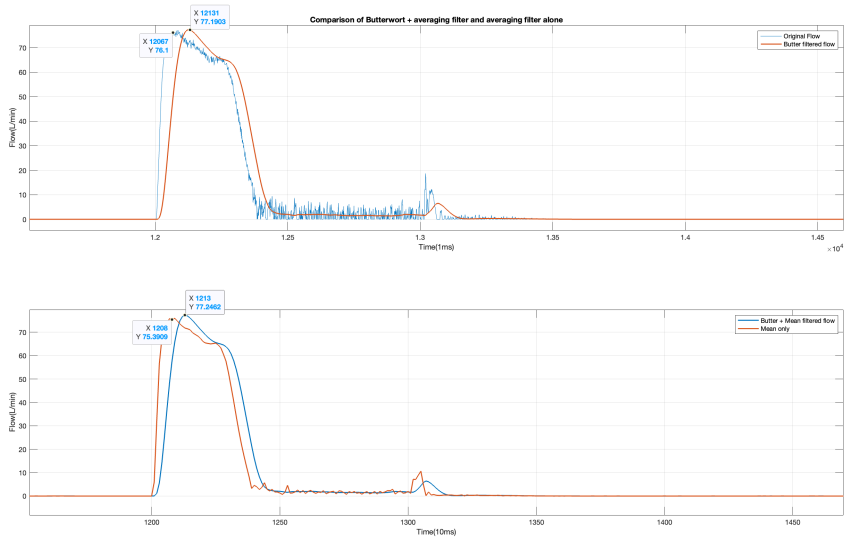

Fig. 4.3: Top: Blue - Unfiltered flow at 1 kHz; Orange - Butterworth-filtered flow at 1 kHz. Bottom: Blue - Butterworth-filtered flow at 1 kHz + 10-point moving average; Orange - 10-point moving average filtered flow.

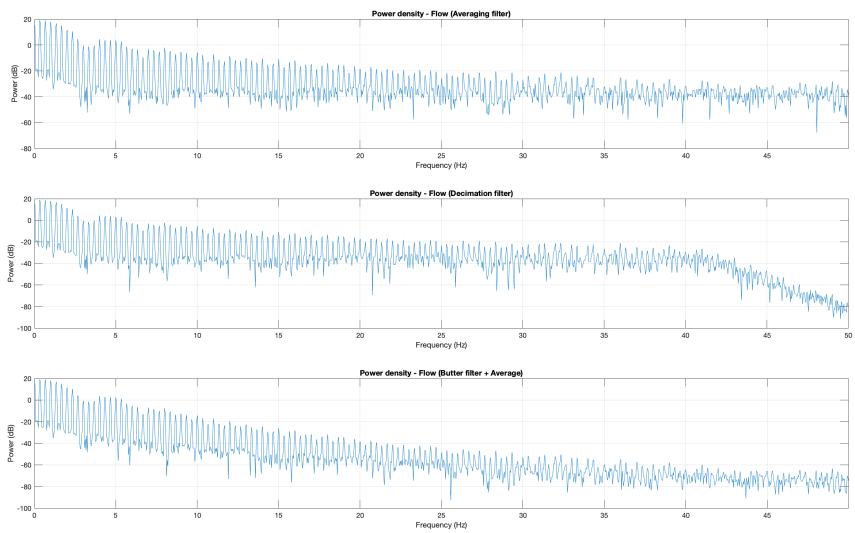

Fig. 4.4: Flow spectral density: Moving average filter, Decimation filter, and Butterworth filter + Moving average filter.

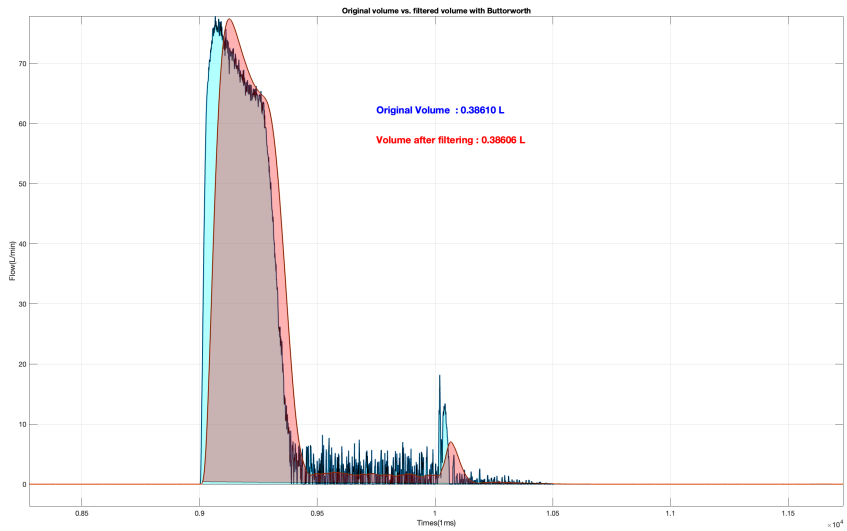

Fig. 4.5: Evaluation of inspired air volume on filtered and unfiltered flow: Blue 0.388610 L (filtered flow), Red 0.388604 L (unfiltered flow), Fr = 20 bpm.

4.1.2.1 Results at Higher Ventilation Frequencies

The performance of the Butterworth filter (1 kHz) combined with the moving average filter was evaluated at ventilation frequencies of 60 bpm and 100 bpm:

- At 60 bpm: The filter effectively preserves the fundamental signal and several harmonics. Noise attenuation beyond the cutoff frequency ($f_c = 3Hz$) remains satisfactory, and the calculated inspired air volume is nearly identical to that of the original data. A 50 ms phase shift is maintained.
- At 100 bpm: Significant limitations were observed. With a fundamental ventilation frequency of 10/6 Hz (1.67 Hz), a cutoff frequency of $f_c = 3Hz$ preserves only two harmonics, causing notable signal distortion. However, the computed inspired air volume remains unchanged, indicating minimal impact on key parameters. A 100 ms phase shift is observed.

4.1.2.2 Filter Adjustment: Cutoff Frequency at 10 Hz

To address the observed distortion at 100 bpm, increasing the cutoff frequency to $f_c = 10Hz$ was proposed. This configuration preserves up to six harmonics of the fundamental signal:

- *Less distorted signal*: The filtered signal profile is significantly improved, closely matching the original data.

- *Inspired air volume*: The computed volumes from filtered and original data remain identical, demonstrating that filtering does not impact essential measurements.
- *Phase shift*: A 50 ms phase shift is observed with a fourth-order filter.

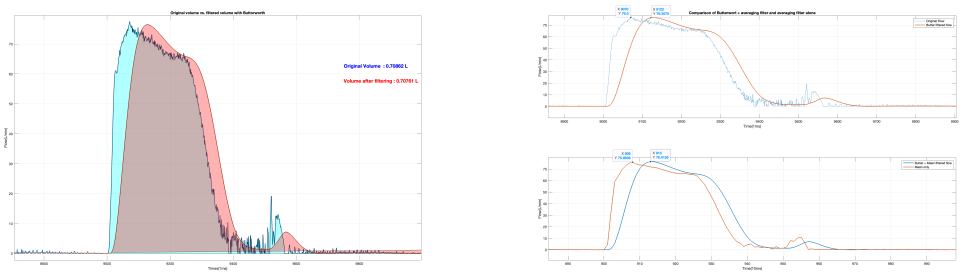

Fig. 4.6: Comparison of inspired volume and phase shift between filtered and original flow, Fr = 60 bpm: Blue 0.70862 L (filtered flow), Red 0.70761 L (unfiltered flow).

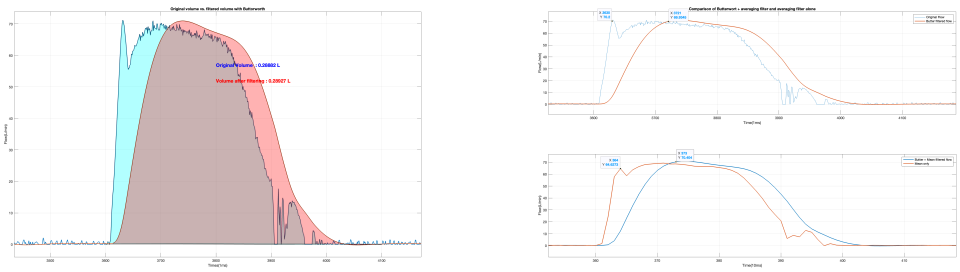

Fig. 4.7: Comparison of inspired volume and phase shift between filtered and original flow, Fr = 100 bpm | $f_c = 3Hz$: Blue 0.28882 L (filtered flow), Red 0.28927 L (unfiltered flow).

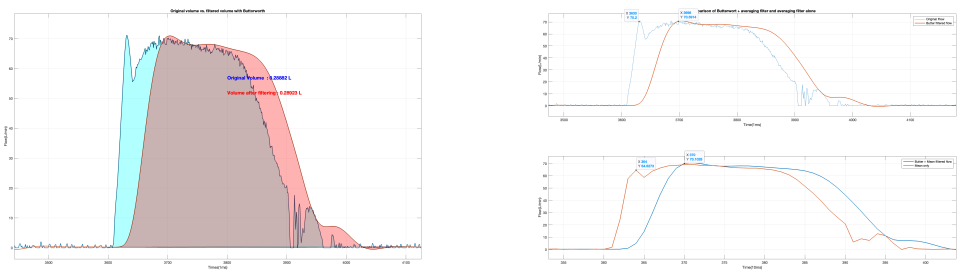

Fig. 4.8: Comparison of inspired volume and phase shift between filtered and original flow, Fr = 100 bpm | $f_c = 10Hz$: Blue 0.28882 L (filtered flow), Red 0.28923 L (unfiltered flow).

4.1.2.3 Conclusion

The combination of a third-order Butterworth filter with a 10-point moving average filter provides significant noise reduction while preserving essential characteristics of ventilation signals. Although filtering introduces a slight phase shift and minor distortion, these effects do not significantly impact critical measurements such as inspired air volume, even at high ventilation frequencies.

4.2 Expiratory Phase

In this section, we analyze the tested actuator, the PSV, focusing on its effective control range in terms of current and its response time.

4.2.1 Static Analysis

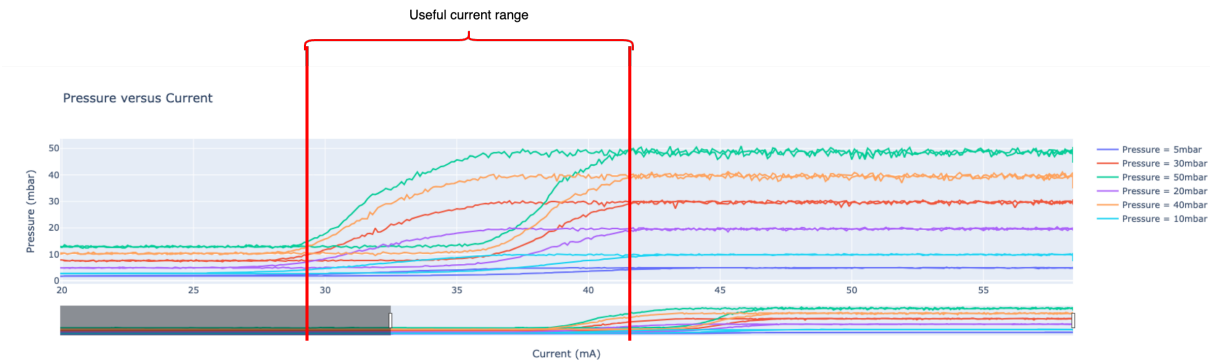

Fig. 4.9: Proximal pressure as a function of current

The plot of command pressure versus control current exhibits hysteresis. This phenomenon is primarily attributed to the magnetic field generated by the current in the PSV. Key observations include:

- *Magnetic Field Effect:* When current is applied to the PSV, an electromagnetic force moves the valve. More force is required to open the valve (increasing pressure) than to close it (decreasing pressure).
- *Current Difference for Opening and Closing:* A higher current is needed to open the PSV during the rising phase than to close it during the descending phase.
- *Control Range*

  The observed control range is between 25 and 43 mA for opening and between 25 and 37 mA for closing. This indicates that the control range is more restricted during closure (decreasing pressure), which limits the flexibility for regulating PEEP during the expiratory phase.

4.2.2 Dynamic Analysis

This test focuses on pressure dynamics, specifically response time. The response times for different test pressures are recorded in the following table:

Table 4.1: Temporal characteristics as a function of pressure

Pressure (mbar)	Rise Time (ms)	Delay (ms)	Response Time (ms)
10	63.5	11	74.5
20	52	9	61
50	41	3	44

4.2.3 PEEP Regulation

With the strategy implemented in 3.7, we tested several levels of PEEP regulation (5, 8, 12, and 15 mbar). The validation criterion used was the slope of expiration, defined as follows (Figure 4.10):

$$\text{Slope} = \frac{\Delta P}{\Delta t} \tag{4.1}$$

The criterion for validation was: $|\text{Slope}| > 40\text{cmH}_2\text{O}$.

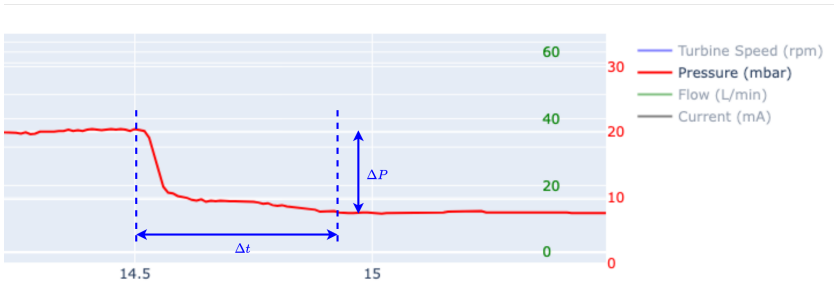

Fig. 4.10: Slope of expiration

Here, we present the results for pressure-controlled ventilation with a peak inspiratory pressure (Pi) of 20 mbar.

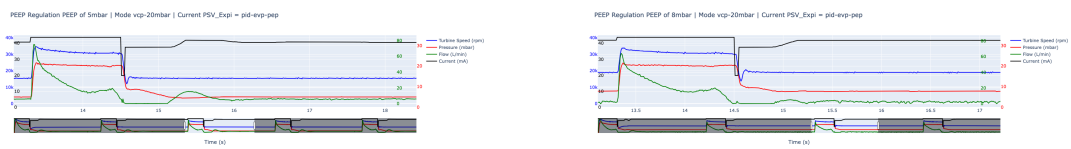

(a) PEEP = 5 mbar (b) PEEP = 8 mbar

Fig. 4.11: Comparison of expiration slopes for PEEP = 5 mbar and PEEP = 8 mbar.

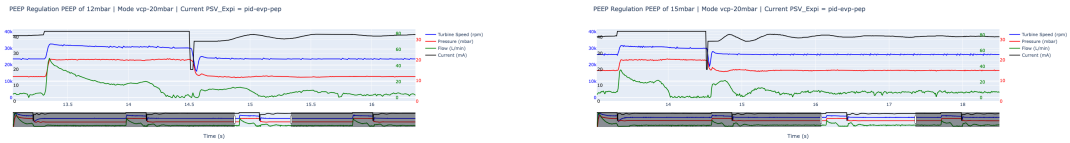

(a) PEEP = 12 mbar (b) PEEP = 15 mbar

Fig. 4.12: Comparison of expiration slopes for PEEP = 12 mbar and PEEP = 15 mbar.

Table 4.2: Slope Expiration for different PEEP levels

PEEP (mbar)	Slope of expiration (cmH_2O/s)
5	25.357
8	40.714
12	167.5
15	102.5

4.3 Inspiratory Phase

In this section, we present the results of pressure regulation using Strategy 1, which involves decoupling speed and pressure regulation. We analyze why this approach was not retained. Subsequently, we introduce cycle-by-cycle regulation strategies and Internal Model Control (IMC).

4.3.1 Decoupling Between Speed and Pressure/Flow Regulation

Turbine speed regulation was performed using a PI controller, as implemented in 2. We then analyzed the delay between the turbine speed profile and the resulting pressure profile for a lung model of type R20C20.

Table 4.3: Comparison of Delay and Rise Time for Different Profiles

Profile	Delay (ms)	Rise Time (ms)
Speed Profile	20	90
Pressure Profile	50	120

We observe a 50 ms delay between the pressure setpoint and the resulting pressure profile from speed regulation. This delay is significantly higher than the 20 ms

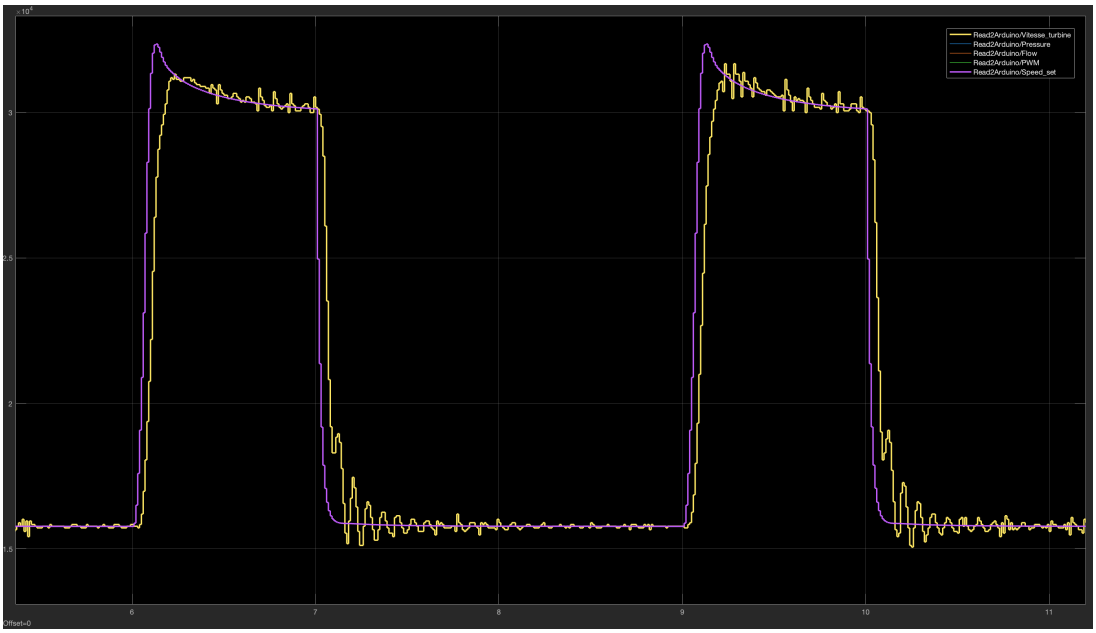

(a) Setpoint speed profile (Purple) and turbine speed (Yellow)

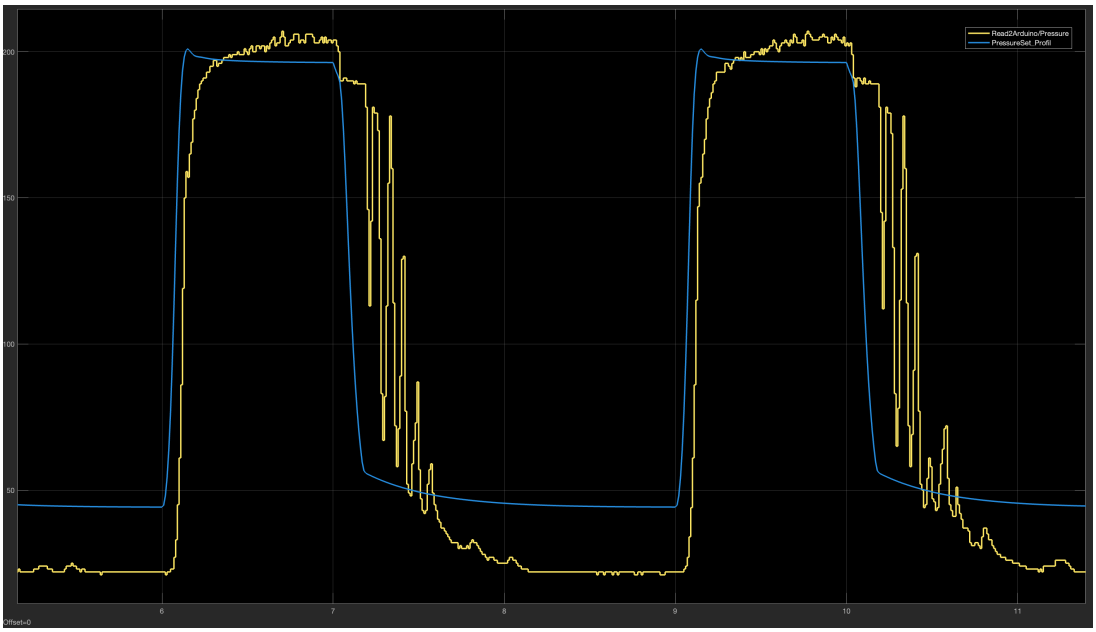

(b) Pressure profile (Blue) and proximal pressure (Yellow) for a peak inspiratory pressure (Pi) of 20 cmH_2O

Fig. 4.13: Comparison of speed and pressure profiles

delay observed with direct pressure regulation. This can be explained by the dual-loop control structure: the high-level pressure regulation introduces a delay, and the subsequent low-level speed regulation further adds to it. The cumulative effect of these delays results in a significant overall delay. Consequently, we conclude that regardless of the speed controller used, the delay will always be higher compared to direct pressure/flow regulation.

4.3.2 PI Controller with Cycle-by-Cycle Adaptation for Pressure/Flow Rate

A PI controller with cycle-by-cycle adaptation, using a coefficient $\alpha = 0.25$, was implemented for direct pressure regulation. The analysis focused on parameters such as slope, steady-state error, overshoot, and stability. The regulation was performed for a peak inspiratory pressure (P_i) of 20 cmH_2O (Figure 4.15).

Table 4.4: Performance Evaluation of Cycle-by-Cycle PI Regulation

Characteristic	Value	Validation
Response Time	145.8 cmH_2O/s	Good
Stability	No oscillations	Good
Accuracy	$P_{proxi} = P_i$	Good
Overshoot	No overshoot	Good

4.3.3 Internal Model Control (IMC)

Internal Model Control (IMC) was implemented for pressure and flow regulation to evaluate its feasibility in this application. This controller relies heavily on the system model, meaning that uncertainties in the model lead to uncertainties in the regulation. The IMC was implemented following the scheme described in Figure 3.24. The model is still in the testing and optimization phase, but initial results are promising.

However, it is evident that for pressure regulation, both flow and turbine speed measurements are required. Consequently, if either of these sensors malfunctions, the regulation will be inaccurate.

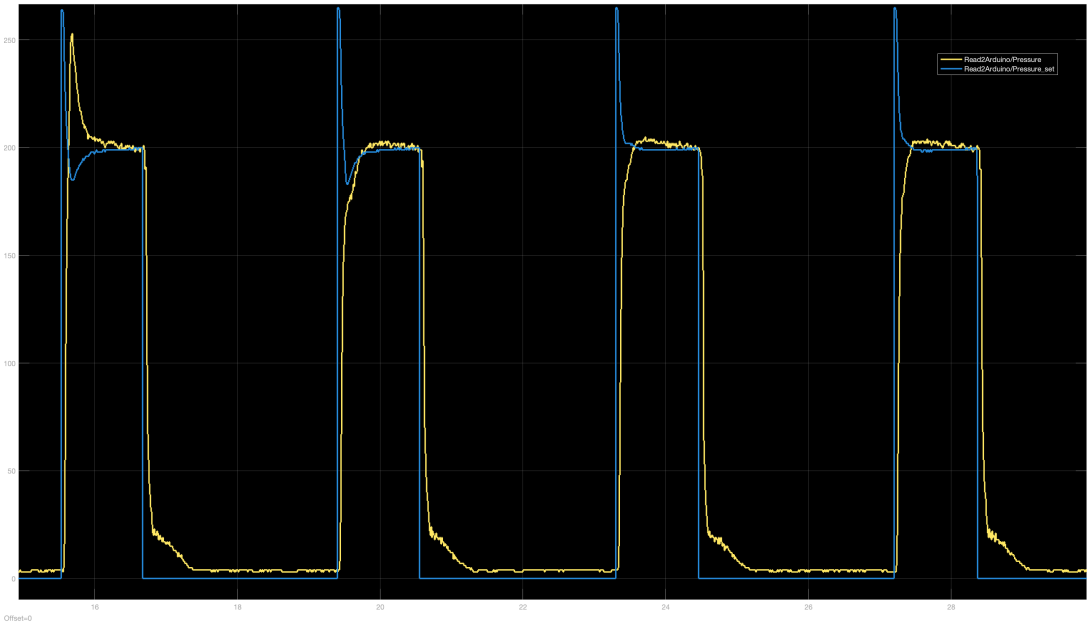

(a) Pressure Setpoint (Blue) and proximal pressure (Yellow) for a peak inspiratory pressure of 20 cmH_2O

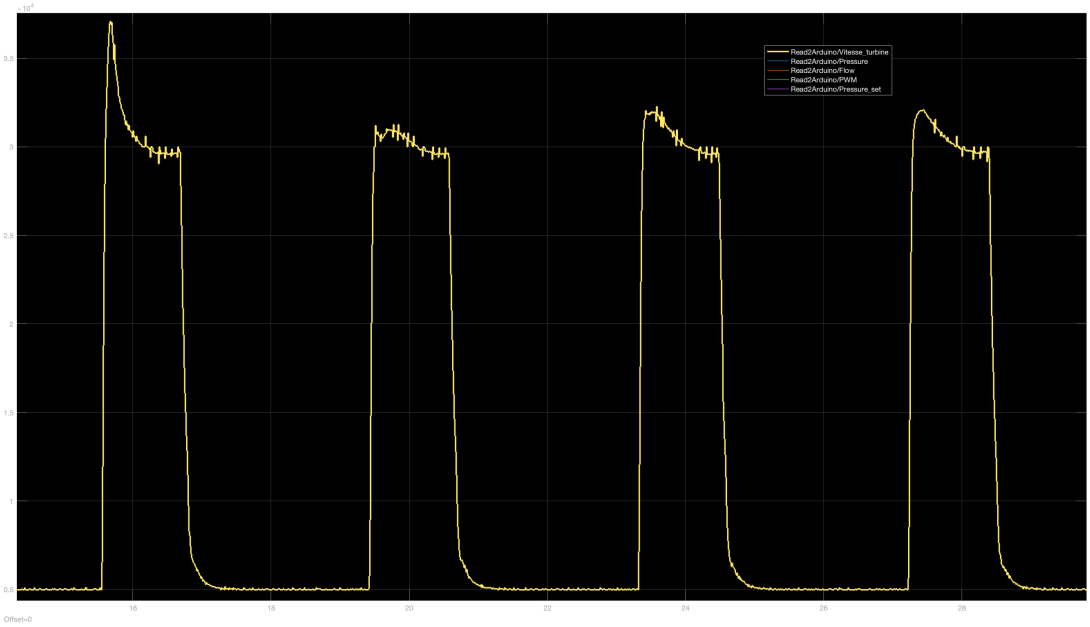

(b) Resulting turbine speed

Fig. 4.14: Cycle-by-cycle PI control results

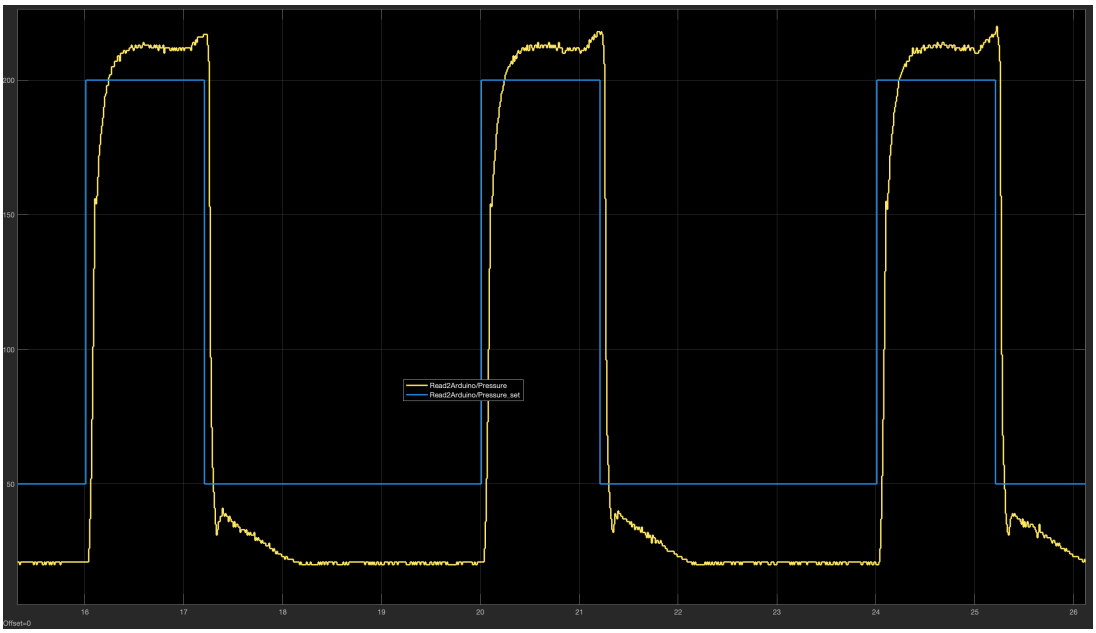

(a) Pressure Setpoint (Blue) and proximal pressure (Yellow) for a peak inspiratory pressure of 20 cmH_2O

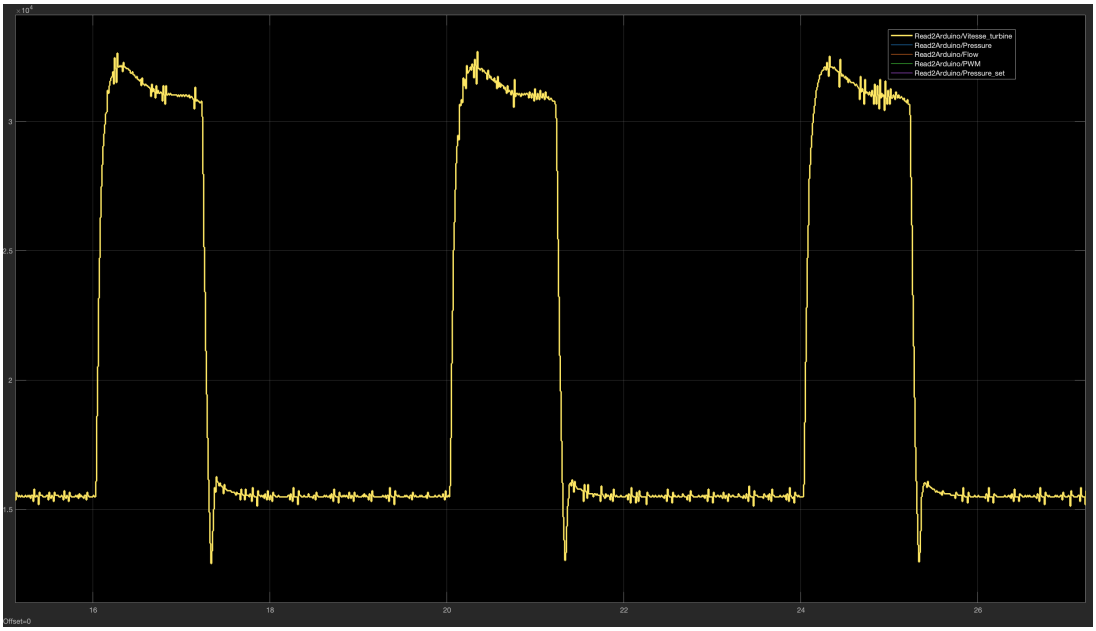

(b) Resulting turbine speed

Fig. 4.15: IMC Control Results

Table 4.5: Performance Evaluation IMC Regulation

Characteristic	Value	Validation
Response Time	109.3 cmH_2O/s	Not Satisfactory
Stability	No oscillations	Good
Accuracy	$P_{proxi} = P_i + 2cmH_2O/s$	Good
Overshoot	No overshoot	Good

Chapter 5

Conclusion and outlook

5.1 Summary

This internship within the Research and Development department was an enriching experience, allowing me to work at the interface between the system design and electronics teams. I had the opportunity to apply and strengthen my skills in modeling and control, particularly by developing MATLAB simulations to test various models and implementing PI and IMC controllers. This work also gave me a better understanding of industrial constraints and the challenges associated with controlling pneumatic turbines used in emergency ventilators.

5.2 Educational Value

From an educational perspective, this internship was particularly instructive. It allowed me to put into practice theoretical concepts studied during my academic training and deepen my knowledge of dynamic system control. Implementing simulations provided me with a better grasp of real system behavior and the limitations of theoretical models. Additionally, working on controller implementation made me more aware of the strategic choices necessary to ensure system stability and performance in a constrained environment.

5.3 Outlook

Several avenues can be explored to further enhance the work carried out. One promising approach would be to investigate a cycle-to-cycle adaptation to optimize control performance, particularly by dynamically adjusting the regulator's coefficients. Regarding IMC, it would be relevant to explore ways to improve model robustness to better adapt to system variations and uncertainties. These perspectives pave the way for future developments that could further enhance the performance and reliability of the control system.

Bibliography

[1] Iron lung - wikipedia https://en.wikipedia.org/wiki/Iron_lung

[2] Canada YL180117 MU MONNAL T60 User Manual (2017), https://www.csrt.com/wp-content/uploads/Canada-YL180117-MU-MONNAL-T60-user-manual-old.pdf

[3] Hess, D.: Respiratory Care: Principles and Practice. Jones Bartlett Learning, Burlington, MA, fourth edition edn. (2020), https://www.jblearning.com/catalog

[4] Morales, S., Palomino, S., Terreros, R., Ulloque, V., Bazán-Lavanda, N., Palacios-Matos, M., Valdivia-Silva, J., Vela, E.A., Canahuire, R.: Pressure and volume control of a non-invasive mechanical ventilator: a pi and lqr approach. In: 2021 9th International Conference on Control, Mechatronics and Automation (ICCMA). pp. 67–71 (2021). https://doi.org/10.1109/ICCMA54375.2021.9646186

[5] Omran, H.: Optimal control (2023), course, Telecom Physique Strasbourg

[6] Reinders, J., Hunnekens, B., Heck, F., Oomen, T., van de Wouw, N.: Adaptive control for mechanical ventilation for improved pressure support. IEEE Transactions on Control Systems Technology **29**(1), 180–193 (2021). https://doi.org/10.1109/TCST.2020.2969381

[7] Soon, H.: Internal model control copyright 2002 internal model control https://www.academia.edu/9405007/Internal_Model_Control_Copyright_2002_Internal_Model_Control

Appendix A

Model Predictive Control for Tracking

Introduction

Model Predictive Control (MPC) is an advanced regulation method that relies on optimizing a system's input over a finite prediction horizon. In the tracking problem, the objective is to minimize the deviation between the actual output $y(t)$ and a reference $r(t)$, while considering the system constraints.

Choice of Input Δu

Instead of using $u(t)$ directly as input, we use the increment $\Delta u(t)$, defined as:

$$\Delta u(t) = u(t) - u(t-1).$$

This approach has several advantages:

- *Reduction of Oscillations*: Increment-based control limits abrupt variations in commands.
- *Numerical Stabilization*: Using $\Delta u(t)$ simplifies optimization as $\Delta u(t)$ is naturally centered around zero.
- *Constraint Handling*: Constraints on $u(t)$ and $\Delta u(t)$ can be formulated more effectively.

By reformulating the input, we augment the system to include $u(t-1)$ in the state $X_a(t)$.

Augmented System Formulation

The original system is given by:

$$\begin{cases} x(t+1) = Ax(t) + Bu(t), & \text{(state equation)} \\ y(t) = Cx(t). & \text{(output equation)} \end{cases}$$

By introducing $\Delta u(t)$, we reformulate the system in an augmented form:

$$\begin{cases} X_a(t+1) = A_a X_a(t) + B_a \Delta u(t), \\ y(t) = C_a X_a(t), \end{cases}$$

where:

$$X_a(t) = \begin{bmatrix} x(t) \\ u(t-1) \end{bmatrix}, \quad A_a = \begin{bmatrix} A & B \\ 0 & I \end{bmatrix}, \quad B_a = \begin{bmatrix} B \\ I \end{bmatrix}, \quad C_a = \begin{bmatrix} C & 0 \end{bmatrix}.$$

Dimensions

- $x(t) \in \mathbb{R}^n$, $u(t) \in \mathbb{R}^m$, $y(t) \in \mathbb{R}^p$,
- $A_a \in \mathbb{R}^{(n+m)\times(n+m)}$, $B_a \in \mathbb{R}^{(n+m)\times m}$, $C_a \in \mathbb{R}^{p\times(n+m)}$.

Cost Function Definition

The objective is to minimize the following cost function over a prediction horizon N:

$$J = \sum_{k=0}^{N-1} \left\{ \|y(t+k) - r(t+k)\|_Q^2 + \|\Delta u(t+k)\|_R^2 \right\},$$

where:

- $Q \in \mathbb{R}^{p\times p}$ weights the deviation $y(t+k) - r(t+k)$,
- $R \in \mathbb{R}^{m\times m}$ weights the control effort $\Delta u(t+k)$.

Using the matrix formulation over the horizon N, this function becomes:

$$J = (Y - r)^T \bar{Q} (Y - r) + Z^T \bar{R} Z,$$

where:

$$Y = \begin{bmatrix} y(t) & y(t+1) & \cdots & y(t+N-1) \end{bmatrix}^T,$$
$$r = \begin{bmatrix} r(t) & r(t+1) & \cdots & r(t+N-1) \end{bmatrix}^T,$$
$$Z = \begin{bmatrix} \Delta u(t) & \Delta u(t+1) & \cdots & \Delta u(t+N-1) \end{bmatrix}^T.$$

Weighting Matrices

$$\bar{Q} = \mathrm{diag}(Q, Q, \ldots, Q) \in \mathbb{R}^{Np\times Np},$$
$$\bar{R} = \mathrm{diag}(R, R, \ldots, R) \in \mathbb{R}^{Nm\times Nm}.$$

Model Matrices

The system dynamics over the horizon is expressed as:

$$X = \bar{S}Z + \bar{K}X_{a0},$$

where:

$$\bar{S} \in \mathbb{R}^{N(n+m)\times Nm}, \quad \text{evolution matrix linked to commands } Z,$$
$$\bar{K} \in \mathbb{R}^{N(n+m)\times(n+m)}, \quad \text{evolution matrix linked to the initial state } X_{a0}.$$

The outputs are given by:

$$Y = \bar{C}X = \bar{C}\bar{S}Z + \bar{C}\bar{K}X_{a0},$$

where:

$$\bar{C} = \mathrm{diag}(C_a, C_a, \ldots, C_a) \in \mathbb{R}^{Np\times N(n+m)}.$$

Substituting Y into the cost function:

$$J = Z^T(\bar{S}^T\bar{Q}\bar{S} + \bar{R})Z + 2\begin{bmatrix} X_{a0}^T & r^T \end{bmatrix}\begin{bmatrix} \bar{K}^T\bar{Q}\bar{S} \\ -\bar{T}\bar{S} \end{bmatrix} Z.$$

Final Optimization Problem

The final optimization problem is:

$$\min_Z J(Z) \quad \text{subject to: } \begin{cases} Z_{\min} \leq Z \leq Z_{\max}, \\ u_{\min} \leq u(t+k) \leq u_{\max}, \quad \forall k \in [0, N-1]. \end{cases}$$

Appendix B

MICADO Datasheet

FORM: JUN 2018

	Unit	min.	typ.	max.	Test	Note
Electrical Data						
Motor Parameters (25°C)						
Phase-Phase resistance	ohm	0.74	0.82	0.90	100%	1,2
Torque constant	mNm/A	3.21	3.49	3.76		1
Back EMF constant	V/Krpm	0.336	0.365	0.394		1
Phase-Phase inductance	mH		0.24			3
Motor constant	mNm/[W]½	3.4	3.8	4.4		1
Rotor inertia	10^{-7} kg.m²		1.3			
Mechanical Time Constant	ms		8.8			
Electrical Time Constant	ms		0.29			
Thermal resistance	°C/W		20			
Dynamic Parameters (25°C) under rated voltage of 24.0 VDC						
No-load						
Current	mA	140	200	260	100%	1
Speed	rpm	60300	65300	71100	100%	1,4
Electrical input power	W	3.4	4.8	6.2		1
Peak efficiency						
Current	A		2.42			
Torque	mNm		7.7			
Speed	rpm		60318			
Electrical input power	W		58.1			
Mechanical output power	W		48.9			
Efficiency	%		84%			
Stall						
Current	A		29.3			
Torque	mNm		102.0			
Electrical input power	W		702.4			
Additional Parameters						
Insulation resistance	MOhm	100.0	OL		100%	1,5
NTC	kOhm	7.0	10.0	11.0	100%	1,6

SCALE 2:1	CREATED BY J. BALLIF	17 Jun 13	ELECTROMAG S.A. Chemin de Bérient CH - 1024 Ecublens
Dimensions and Tolerances in mm	MODIFIED BY F. GIGON	11 Jan 19	TITLE Outline drawing
General Tolerances: ISO 2768-fH	APPROVED BY E. BALLIFARD	10 Mar 20	SIZE A3 / PART NO 200A0123 / REV B00
This drawing contains confidential information and is issued in confidence on the conditions that it be returned on demand and not be copied, reproduced, disclosed to others or used without the written consent of ELECTROMAG S.A.			PROJECT NO. RD12/501 / SHEET 3 OF 5

Fig. B.1: Datasheet of MICADO